Slab failure or slab success? Examining the contributions of crust and mantle to post-subduction magmatism in the Ratagain Complex, NW Scotland

Lawrence, Anya; Fowler, Mike; Kingsbury, Cole; Knott, Tom ; Mark, Darren ; Stevenson, Carl

DOI:
10.1016/j.lithos.2023.107139

Document Version
Publisher's PDF, also known as Version of record

Citation for published version (Harvard):
Lawrence, A, Fowler, M, Kingsbury, C, Knott, T, Mark, D & Stevenson, C 2023, 'Slab failure or slab success? Examining the contributions of crust and mantle to post-subduction magmatism in the Ratagain Complex, NW Scotland', *Lithos*, vol. 448–449, 107139. https://doi.org/10.1016/j.lithos.2023.107139

LITHOS 448-449 (2023) 107139

Contents lists available at ScienceDirect

LITHOS

journal homepage: www.elsevier.com/locate/lithos

Slab-failure or Slab-success? Examining the contributions of crust and mantle to post-subduction magmatism in the Ratagain Complex, NW Scotland

A. Lawrence [a,*], M. Fowler [b], C.G. Kingsbury [c], T. Knott [d], Darren Mark [e], C.T.E. Stevenson [a]

[a] School of Geography, Earth and Environmental Sciences, University of Birmingham, Birmingham B15 2TT, UK
[b] School of the Environment, Geography and Geosciences, University of Portsmouth, Burnaby Road, Portsmouth PO1 3QL, UK
[c] Faculty of Geology and Geography, National Research Tomsk State University, Lenin Avenue, 36, Tomsk, Tomsk Oblast 634050, Russian Federation
[d] SciMed, Unit B4, The Embankment Business Park, Vale Road, Heaton Mersey SK4 3GN, UK
[e] Scottish Universities Environmental Research Centre, Rankine Avenue, East Kilbride G75 0QF, UK

ARTICLE INFO

Keywords:
Granite
High Ba-Sr
Slab break-off
Caledonian
Crystal mush
Crustal contamination

ABSTRACT

The Ratagain Complex is an enigmatic Late Caledonian granitic intrusion and a member of the high Ba—Sr Northern Highlands granite (NHG) suite that has been related to slab failure. Slab failure magmatism explains varying contributions of mafic and felsic magmas in post-collision orogenic settings. It is therefore of major importance in understanding crustal accretion. However, the source and nature of any mantle derived contribution is poorly understood. This study reveals that Ratagain is not only transitional in nature between the high Ba—Sr calc-alkaline granites and syenite intrusions of the Northern Highlands Terrane, but overlaps with the entire compositional range of the NHG suite. New lithogeochemical data from Ratagain confirm remarkably high Sr (>1600 ppm) and Ba (>2200 ppm) contents, high LREEs, notable depletions in Nb, U, P and Ti, low HREEs and negligible Eu anomalies, associated with high initial $^{87}Sr/^{86}Sr$ (0.7055 to 0.7062) and low εNd (− 11.8 to −13.3). Although mafic parts of the complex have strong elemental and isotopic similarities with broadly coeval lamprophyres, signalling derivation from enriched mantle sources, details of the isotope array with respect to local crustal reservoirs indicate a significant Lewisian component. Such geochemical characteristics, combined with tectonic and petrological evidence, may be attributable to long-lived, incremental emplacement of successive magma batches originating from the same enriched mantle but differing in age and extent of assimilation-fractionation crystallisation. We therefore propose that some of the age dates for the Late Caledonian intrusions, particularly those obtained from older geochronology studies, are in need of review as they may record early crystallisation in the deep crust and not be a valid proxy for granite emplacement.

1. Introduction

Granites are the primary component of the upper continental crust. Therefore, understanding how granitic magmas are generated is key to understanding how the Earth's continental crust has grown throughout geological time. Whilst traditional arguments centre on arc-derived magmatism to account for the presence of granites and related rocks with compositions >60% SiO_2 in the continental crust (Rudnick, 1995; Lee et al., 2007; Hawkesworth et al., 2009), the more recent and increasingly popular paradigm is that intermediate-felsic magma is formed during the closing stages of continental collision and ensuing rupture and separation of subducting plates during such collisions (Atherton and Ghani, 2002; Hildebrand et al., 2018; Macera et al., 2008).

Late Caledonian intrusive complexes in Scotland have offered a long-standing opportunity to study the growth of continental crust by the emplacement of granitic bodies. These granites (sensu *lato*) were generated during the late stages of the Caledonian Orogeny, a major crust-forming episode which took place between the Cambrian (c. 500 Ma) and early Devonian (c. 360 Ma) (MacDonald and Fettes, 2006) and involved the convergence of the three palaeocontinents of Laurentia, Baltica and Avalonia (Stephenson et al., 1999).

The Late Caledonian granites are interpreted to have formed in the Silurian and Devonian, following the subduction of the Iapetus oceanic

* Corresponding author.
E-mail address: a.lawrence.2@bham.ac.uk (A. Lawrence).

https://doi.org/10.1016/j.lithos.2023.107139
Received 17 May 2022; Received in revised form 16 March 2023; Accepted 17 March 2023
Available online 31 March 2023

crust beneath Laurentia. Research over several decades has provided a detailed account of the petrogenesis and structural emplacement of the granitoids. However, the models emerging from this work have been the subject of much debate. This is partly because the rocks have several subduction-related characteristics (Harmon et al., 1984; Pidgeon and Aftalion, 1978; Thompson and Fowler, 1986) yet their spatial distribution, age and geochemistry cannot be ascribed to active subduction of Iapetus Oceanic crust (Atherton and Ghani, 2002; Miles et al., 2016).

Atherton and Ghani (2002) were the first to link post-subduction Late Caledonian magmatism to a 'slab break-off' event, suggesting that oblique continental convergence following the subduction of the Iapetus oceanic crust caused the subducted plate to weaken, rupture and detach near the oceanic-continental crust interface, leaving a 'gap' at the base of the mantle lithosphere. The rise of hot, dry asthenosphere to fill this gap initiated partial melting in the overlying subcontinental lithospheric mantle (SCLM) and underplated lamprophyric magma was formed. Some of this early, mafic magma was emplaced at high crustal levels as lamprophyre-appinite dykes in the middle-Silurian (c. 430 Ma) (Atherton and Ghani, 2002; Neilson et al., 2009). Continued asthenospheric upwelling, replacement and sustained high temperatures at the base of the mantle lithosphere as the detached slab sank away subsequently caused partial melting of the early lamprophyric underplate, generating magmas with unusual trace element-signatures (high Ba, Sr and LREE contents) characteristic of the Late Caledonian granites (Atherton and Ghani, 2002). Subsequent magmatic differentiation was achieved through assimilation-fractional crystallisation (AFC) processes involving different crustal reservoirs (Fowler et al., 2008; Fowler and Rollinson, 2012).

Since it was first suggested by Atherton and Ghani (2002), the slab break-off model (which perhaps should be considered a 'success' in terms of granitic magmatism) has been refined step-by-step by various authors to account for the elemental peculiarities and considerable volumes of granitic magmas emplaced post-collision in the British Caledonian (Archibald and Murphy, 2021; Dewey et al., 2015; Miles et al., 2016; Neilson et al., 2009; Oliver et al., 2008). Archibald et al. (2022) provide further confirmation of this hypothesis, by comparison of compiled elemental data with the slab failure discrimination diagrams of Hildebrand et al. (2018) and Whalen and Hildebrand (2019).

This study presents new field, petrographical and geochemical data for the Ratagain Complex, an under-studied granitic intrusion in north west Scotland, whose petrogenesis has been ascribed to slab break-off processes based on regional synthesis of the Late Caledonian suite (Archibald et al., 2022; Fowler et al., 2008; Fowler and Rollinson, 2012; Miles et al., 2016). Our sizeable geochemical dataset (>100 samples from a single pluton) provides further constraints on potential source regions for Late Caledonian high Ba—Sr intrusions, mechanisms of magmatic evolution and the relative importance of mantle and crustal components in the wider context of slab failure and post-collision mafic magmatism.

2. Geological background

2.1. Caledonian Orogeny

Caledonian granites, such as those that make up the Ratagain Complex, were generated during the Caledonian Orogeny, the crust-forming episode that is largely responsible for the present-day configuration of terranes and terrane-bounding faults in the British Isles (McKerrow et al., 2000; Searle, 2022). The orogeny resulted from the closure of the Iapetus Ocean and the subsequent convergence of Laurentia (which is represented today largely by the Precambrian basement rocks of North America, Greenland, north of Ireland and Scotland), Baltica (Scandinavia and Russia) and Avalonia (the basement of southern Ireland, Wales and England) (e.g. Kinny et al., 2003; Goodenough et al., 2011; Strachan et al. 2020; Searle, 2022). As well as causing considerable deformation and crustal thickening, the Caledonian Orogeny was accompanied by an extended period of magmatism in the British Isles and the Caledonian igneous rocks have a variety of compositions and modes of emplacement (Stephenson et al., 1999).

2.2. Caledonian magmatism

Caledonian magmatism in Britain and Ireland mainly occurred in two episodes. The first was the Mid-Ordovician Grampian event (c. 470–460 Ma), a phase of arc–continent collisions along the southern margin of Laurentia (Johnson et al., 2017; Oliver et al., 2008). The later magmatic episode took place during the Late Silurian–Early Devonian (c. 447–383 Ma) as the Iapetus Ocean finally closed (Dewey et al., 2015). In Scotland, this magmatism was marked by volcanic activity in the Midland Valley and Southern Uplands, regional dyke swarms, and the emplacement of granitic intrusions across large areas of the country, especially the Grampian and Northern Highlands.

Read (1961) first categorised the Caledonian granitic intrusions as the 'Older Granites' and 'Newer Granites'. The Older Granites are two-mica S-type granites (Oliver et al., 2008) which, together with an associated suite of gabbroic rocks (the Newer Gabbros), are representative of *syn*-collisonal magmatic activity that took place in the Mid-Ordovician Grampian event (Brown et al., 2008).The Newer Granites (hereafter Late Caledonian granites) are a much larger group of over one hundred intrusions, including sheets, veins and plutons varying in areal extent from 1 to 380 km^2, with mostly I-type but also some S-type affinities (Fig. 1; MacDonald and Fettes, 2006). The Late Caledonian granites are typically associated with mantle-derived lamprophyres and appinites (Rock et al., 1988) and yield Rb—Sr and U—Pb ages between c.435–390 Ma (Soper, 1986). This period encompasses the closure of the Iapetus Ocean (c. 435–425 Ma), the Scandian collision of Laurentia and Baltica, the collision of Laurentia and Eastern Avalonia and Acadian regional sinistral shear deformation (Archibald and Murphy, 2021; Lancaster et al., 2017; Rogers and Dunning, 1991).

2.3. The Late Caledonian granites

On the basis of isotope and geochemical characteristics, Stephens and Halliday (1984) categorised the Late Caledonian granites into the Argyll, Cairngorm and South of Scotland suites, the latter of which was later divided into the South of Scotland and Galloway subgroups by Highton (1999). However, Brown et al. (2008) recognised that the Galloway subgroup had compositional similarities to granites in northern England, the Isle of Man and western Ireland and thus they amalgamated all of these granitoid intrusions into a single group named the Trans-Suture Suite.

The Argyll and Northern Highlands Suite consists of hornblende-granodiorite, biotite-granodiorite and syenite plutons with dioritic and monzo-granitic components (MacDonald and Fettes, 2006) together with spatially and temporally associated appinites. The rocks of this suite are characterised by relatively high Ba—Sr concentrations (Fowler et al., 2008), which are discussed below.

The Cairngorm Suite is dominated by biotite-monzogranite plutons (Stephens & Halliday, 1984) and when compared to the granitoids of the Argyll and Northern Highlands Suite, they have lower Ba and Sr abundances and intermediate and appinitic rocks are scarce. The South of Scotland and Trans-Suture suites comprise composite granodiorite and pyroxene diorite plutons, which are richer in K and Th than the other suites (MacDonald and Fettes, 2006). Nevertheless, like the Cairngorm Suite, they have relatively low Ba—Sr contents.

2.4. High Ba—Sr granites

First recognised by Tarney and Jones (1994), high Ba—Sr granites are characterised by extreme enrichment in barium (Ba) and strontium (Sr). In addition to high Ba and Sr (>1000 ppm) Mg#, Cr, V and Ni contents, high Ba—Sr granites can also be distinguished from traditional

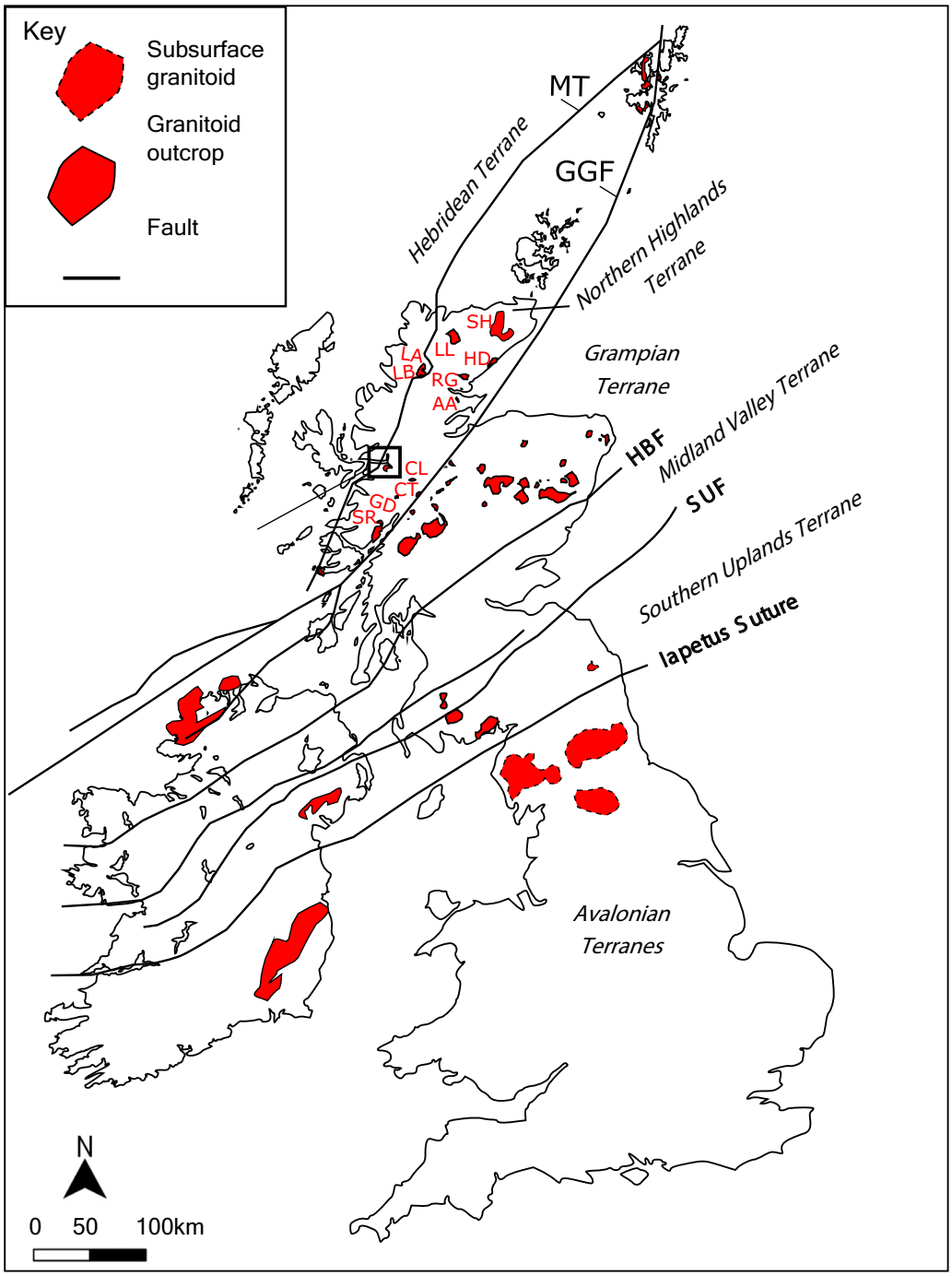

Fig. 1. Overview map of the Late Caledonian Silurian-Devonian granitoids of Great Britain and Ireland adapted from Brown et al. (2008) and Fowler et al. (2008). The box Fig. 2 highlights the location of the Ratagain Complex. High Ba—Sr intrusions mentioned in the text are labelled in red. Key to abbreviations: AA is Ach'Uaine Appinites; CL is Cluanie; CT is Clunes tonalite; GD is Glen Dessary; GGF is Great Glen Fault; HBF is Highland Boundary Fault; HD is Helmsdale; LA is Loch Ailsh; LB is Loch Borralan; LL is Loch Loyal; MT is Moine Thrust; SH is Strath Halladale; SR is Strontian; SUF is Southern Uplands Fault; RG is Rogart. (For interpretation of the references to colour in this figure legend, the reader is referred to the web version of this article.)

I-, S- and A-types (Fowler et al., 2001) owing to their absent or small negative Eu anomalies, LREE (light rare earth elements) and LILE (large ion lithophile elements) enrichment, and relatively low HFSE (high field strength elements) contents (Tarney and Jones, 1994).

Whilst high Ba—Sr granites have been described in other locations in the world, such as the Tibetan Plateau (Ye et al., 2008) and central Brazil (Leite et al., 2021), the Northern Highlands of Scotland are a type locality for this group. The Late Caledonian high Ba—Sr suites of the Northern Highlands (hereafter 'NHG suite') can be divided, on the basis of petrographic and geochemical criteria, into two subgroups: (1) alkaline syenitic plutons that crop out in the west and (2) calc-alkaline granitic plutons in central and eastern areas (Fig. 1; Bruand et al., 2014).

2.5. The Ratagain Complex

The Ratagain Complex is a Late Caledonian granitic intrusion which crops out along the shores of Loch Duich in the western Highlands of Scotland (Hutton et al., 1993; Fig. 2). The intrusion is hosted by metasedimentary rocks of the Neoproterozoic Morar Group and the Archean-Paleoproterozoic Lewisian Gneiss basement of the Eastern Glenelg inlier (Krabbendam et al., 2018). Biotite- and feldspar-whole-rock ages of 415 ± 5 Ma (Turnell, 1985) and 419 ± 3 Ma (Thirlwall, 1988) are reported for the complex, whilst U—Pb zircon and baddeleyite dating places the emplacement at 425 ± 3 Ma (Rogers and Dunning, 1991).

Although loosely termed 'granitic', the Ratagain Complex is composed of a variety of intrusive units besides granite, such as syenite, monzonite, monzodiorite (Hutton and McErlean, 1991) and can thus be

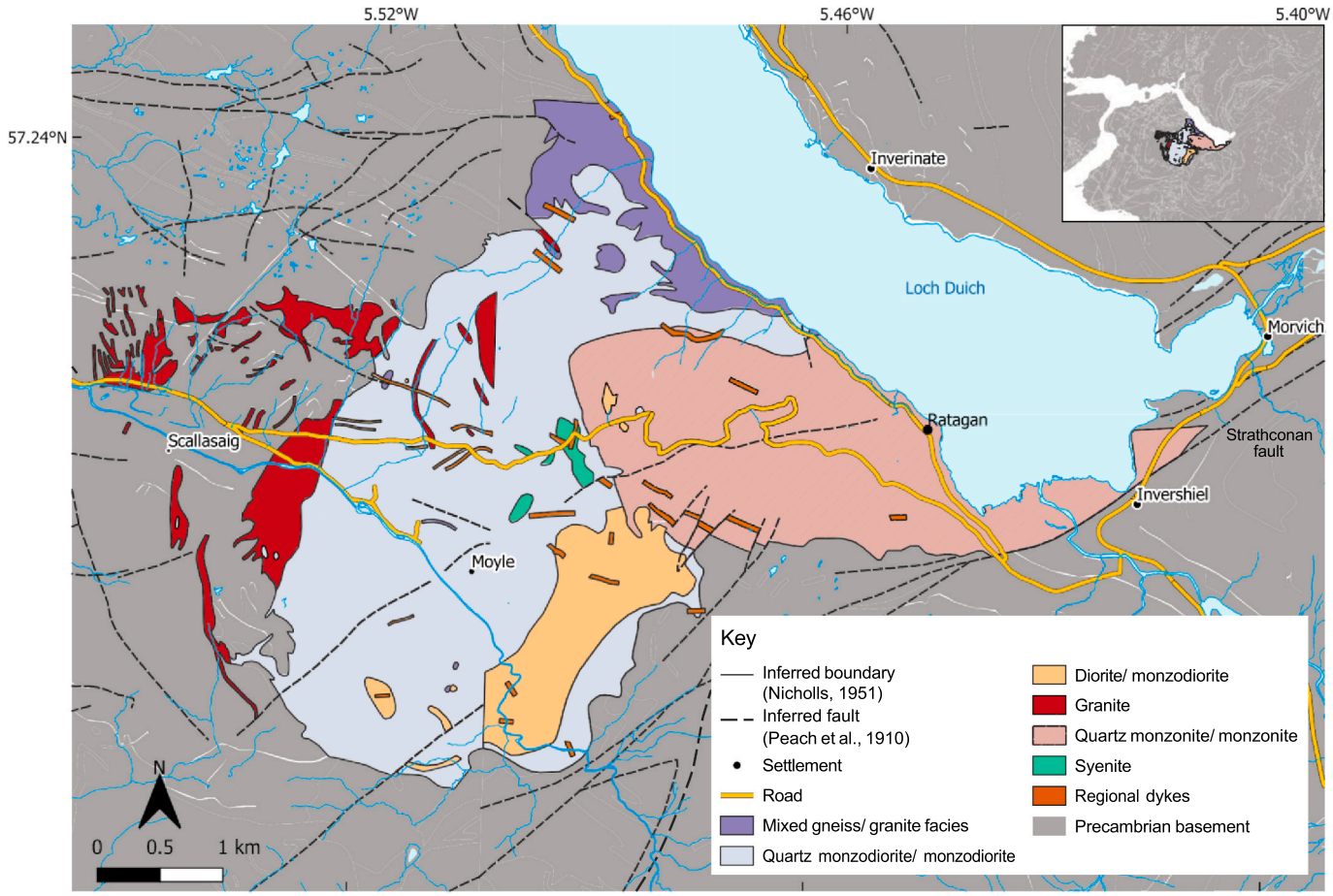

Fig. 2. Simplified geological map of the Ratagain Complex reproduced from Lawrence et al. (2022). Locational information for all 112 sampling sites is provided in Supplementary Table SA2.

considered as compositionally transitional between the Late Caledonian alkaline syenites and the more common metaluminous calc-alkaline granites (Fowler et al., 2008). According to Fowler et al. (2008), the calc-alkaline granites of the NHG suite evolved by amphibole and plagioclase-dominated fractionation involving contamination with Moine metasedimentary rocks, whilst the syenites resulted from biotite-pyroxene-dominated fractionation accompanied by assimilation of Lewisian granulite-facies gneisses.

Ratagain also exhibits elemental characteristics typical of high Ba—Sr intrusives, notably: extreme enrichment in Ba, Sr and the light REEs (Stephenson et al., 1999); enrichment in the alkalis, especially Na and K (Alderton, 1988); and relatively low HFSEs including distinct negative Nb—Ta anomalies (Fowler et al., 2008).

Whilst the Ratagain Complex has already been the subject of a comprehensive rock magnetic study (Lawrence et al., 2022), chemical and isotopic data for the intrusion are somewhat lacking in the literature (Fowler et al., 2008; Thompson and Fowler, 1986). Therefore, although the Ratagain Complex's distinctive abundance of mafic-intermediate compositions and transitional nature could likely inform the Late Caledonian tectonic regime (e.g. Fowler et al., 2008; Hutton et al., 1993; MacDonald and Fettes, 2006; Stephenson et al., 1999), a more robust geochemical dataset is required to better understanding of the intrusion's petrogenetic and tectonic implications in the context of the British Caledonides.

3. Sampling and analytical methods

112 block samples, ranging from 1 to 5 kg in weight, were collected and prepared for geochemical analysis at the University of Birmingham. Preparations included removing all visibly weathered surfaces from the block samples and cutting a rectangular fragment, approximately 100 mm × 50 mm in dimensions, from each block sample. Coarse crushing of the fragments was achieved using a jawcrusher, whilst further crushing to yield fine powders (200 mesh) was undertaken on a tungsten-carbide TEMA T750k laboratory disc mill.

Petrographic classification of all samples was made on the basis of thin section observations and X-ray fluorescence (XRF) major and minor elemental analyses. XRF analyses were undertaken at the University of Portsmouth using pressed powder pellets. Pressed powder pellets were prepared by combining 5 g of powdered rock sample and 1 g of CEREOX® binder and then placing the sample in a tungsten carbide die. The die was compressed for 30 s under a manual press with 21 tons of applied pressure. Estimates for loss on ignition (LOI) were made after heating 1 g of sample in an oven at 1000 °C for 1.5 h, cooling and reweighing.

Ten major element oxides (SiO_2, TiO_2, Al_2O_3, Fe_2O_3, MnO, MgO, CaO, Na_2O, K_2O and P_2O_5) and nineteen trace element compositions (Sc, V, Cr, Ni, Cu, Zn, Ga, Rb, Sr, Y, Zr, Nb, Ba, Pb, La, Ce,Th, U and Sn) were analysed using a Rigaku Primus ZSX II WDXRF spectrometer with instrumental lower limits of detection of ca. <10 ppm. Precision and accuracy were monitored using the standards JB-1A and JG-1A and are estimated at ca. <2% for major elements and ca. <5% for trace elements. The rare earth element (REE) compositions of 40 samples were analysed through inductively coupled plasma mass spectrometry (ICP-MS, Analytic Jena PQ Elite) following fusion dissolution with a lithium metaborate flux, also at the University of Portsmouth. Accuracy and precision were analysed routinely with the same CRMs, estimated to be ca <5%. For full major and trace element XRF data see Supplementary

table SA2; for LOI estimates see Supplementary table SA3.

5 samples were also analysed for Sr and Nd radiogenic isotope compositions at the Scottish Universities Environmental Research Centre (SUERC), East Kilbride, Scotland on a VG Sector 54–30 thermal ionization mass spectrometer (TIMS). $^{87}Sr/^{86}Sr$ was corrected for mass fractionation using $^{86}Sr/^{88}Sr = 0.1194$. Repeat analysis of the NIST SRM-987 Sr standard gave 0.710257 ± 17 (2 sd, $n = 10$) for the duration of this study (see Troll et al., 2019 for full analytical details). The decay constant used was (σ) 1.42×10^{-11} (Steiger and Jäger, 1977) to determine the initial Sr isotope ratios (see Supplementary Table SB1).

$^{143}Nd/^{144}Nd$ was corrected for mass fractionation using $^{146}Nd/^{144}Nd = 0.7219$. During the course of this study, the SUERC internal Nd laboratory standard (JM), which is calibrated against the La Jolla Nd solution and the JNdi-1 standard, gave $^{143}Nd/^{144}Nd = 0.511511 \pm 8$ (2 sd, $n = 8$). To estimate initial isotope ratios the decay constant used was (σ) 6.54×10^{-12} (Lugmair and Marti, 1978). Chondritic Uniform Reservoir (CHUR) modelling (De Paolo, 1988) was used to compare the initial isotopic compositions of the Ratagain Complex samples with that of primitive mantle at the time of their generation. The assumed present-day values for CHUR were $^{147}Sm/^{144}Nd = 0.1967$ and $^{143}Nd/^{144}Nd = 0.512638$ (Jacobsen and Wasserburg, 1980; see also Supplementary Table SB2).

Finally, single crystal major element data for 5 representative samples were obtained using a Zeiss SIGMA 300VP Scanning Electron Microscope (SEM), at the University of Leicester, equipped with two Bruker XFlash 6|60 energy-dispersive X-ray detectors (EDX) with 126-eV energy resolution. A high-resolution back-scattered electron (BSE) contrast image was collected at each site of interest in order to accurately locate analytical points (typically cores and rims in selected mineral phases). Quantitative analyses were performed using a 15 kV beam acceleration and a 60 μm aperture providing a 10 nA beam current. Dwell time at each analytical point was fixed at 20 s, generating a spectra with >1,000,000 counts for accurate deconvolution. Quantification utilised a Phi-Rho-Z correction routine and resultant element concentrations are reported as normalized weight percent (wt%). Simultaneous analyses of MAC reference minerals (Albite, Orthoclase, Hornblende) indicate that precision for the observed data range over the period of analytical work was typically better than 3% (1σ – RSD) whilst accuracy was typically better than 5% (see Supplementary table SC1).

4. Results

4.1. Geology and petrography

For a detailed account on key field relationships and features of the Ratagain Complex, the reader is referred to Lawrence et al. (2022). The new whole-rock geochemical data (Table 1) presented in this study confirm that the Ratagain Complex is markedly heterogeneous in composition. The lithological names assigned to the rock compositions we analysed are based on their CIPW normative mineralogy (Fig. 3). It can thus be seen that the Ratagain complex is dominated by quartz monzonite and quartz monzodiorite, but granite, monzonite, monzodiorite, granodiorite and syenite facies also crop out within the mapped boundaries of the intrusion.

Igneous textures vary from fine-grained and equigranular (Fig. 4D) to medium-grained (Fig. 4A, C, E) to coarse-grained and porphyritic (Fig. 4F). Mafic microgranular enclaves (MMEs) ranging from a few cm up to 5 m in size (Fig. 4B, C) occur in all facies of the Ratagain Complex; such features are suggestive of magma mixing and mingling processes involving juvenile mafic to ultramafic material (Fowler et al., 2008).

The typical felsic mineralogy of the granite, granodiorite, quartz monzonite, monzonite, quartz monzodiorite and monzodiorite is characterised by quartz, plagioclase and alkali feldspars in variable proportions. Plagioclase occurs in high abundances as elongate, euhedral crystals often showing multiple twinning, perthitic textures and zoning, whilst alkali feldspar occurs in lower abundances as tabular crystals showing simple twinning (Fig. 5C, D). Both are intergrown with ubiquitous irregular, anhedral crystals of quartz (Fig. 5A, B). Sericitization of the feldspars occurs to varying degrees across all samples (Fig. 5A-D). Mafic minerals, which may include biotite, hornblende and relict clinopyroxene (Fig. 5E, F), occur in lesser proportions and usually show partial or complete alteration to chlorite.

In the Ratagain syenite however, mafic phases dominate the mineralogy and appear markedly fresher and less affected by alteration than in the other facies (Fig. 5G, H). Biotite occurs as elongate lamellae or plates, with some crystals hosting opaque inclusions and dark pleochroic zircon haloes. Clinopyroxene is present as equidimensional crystals, the latter of which typically show prominent cleavage intersections at 90° and simple twinning in some cases. Hornblende occurs as prismatic or lozenge-shaped euhedral crystals which display prominent 120° cleavage intersections and/or zoning.

The accessory mineralogy of all facies is characterised by mixtures of titanite, apatite, zircon, zoisite and/or opaque minerals (Fe—Ti oxides), which are interpreted as primary owing to their partial to complete encompassment by the main mafic minerals. Apatite occurs as small, high-relief, euhedral crystals or inclusions within biotite, hornblende and the feldspars. Crystals have a cloudy interior and dark rim. Titanite is present as small, rectangular lozenges and less common diamond-shaped crystals (Fig. 5A, B). Rare bladed and acicular crystals of zoisite, distinguished by their high-relief, are evident in some studied samples.

4.2. Major and trace element data

XRF major and trace elemental data for all 112 samples are reported in the Supplementary Material (Supplementary table SA2). Representative whole-rock major and trace element data for the Ratagain Complex are presented in Table 1.

The alumina saturation index of Maniar and Piccoli (1989) demonstrates that the facies are mostly metaluminous in nature, with only a small number of the granitic-granodiorite and quartz monzodiorite-monzodiorite facies showing a slightly peraluminous affinity (Fig. 6A). All the studied intrusives mainly plot in the magnesian series (Fig. 6C) of Frost et al. (2001) and can be classified as non-tholeiitic according to Irvine and Baragar (1971) AFM diagram (Fig. 6B). The MALI (Modified Alkali-Lime index) versus SiO_2 diagram of Frost et al. (2001) (Fig. 6D), indicates that both the quartz monzodiorite-monzodiorite facies and quartz monzonite facies mostly fall within the alkalic domain, whilst the monzonite and granite-granodiorite facies mainly plot across the alkalic and alkali-calcic fields.

Variation diagrams demonstrate that the SiO_2 concentrations for the various intrusive units of the complex range from a minimum of 43.60 wt% for a monzonite sample to a maximum of 81.92 wt% in a quartz-rich granitoid sample. In all intrusive units, SiO_2 correlates negatively with TiO_2 (0.26–2.42 wt%, Fig. 7A), Fe_2O_3 (0.91–13.5 wt%, Fig. 7B), MnO (bdl - 0.14 wt%, Fig. 7D), MgO (0.14–9.57 wt%, Fig. 7E) and CaO (0.48–13.87 wt%, Fig. 7F). Al_2O_3 (Fig. 7C) shows the characteristic convex-up distribution delineating a positive correlation from ca. 40 to ca 65 wt% silica, then a negative correlation towards the silicic extremes. Na_2O (2.17–6.91 wt%, Fig. 7G) and K_2O(1.47–8.06 wt%, Fig. 7H) are rather scattered across SiO_2 concentrations but both elements generally mimic Al_2O_3, with highest values close to 65% SiO_2.

Data for trace elements are also presented as Harker-style plots for a selection of LILEs, transition metals and HFSEs to illustrate the variation within the suite (Fig. 8). The rocks of the Ratagain Complex exhibit remarkably high Sr and Ba abundances, which can reach up to 4101 ppm and 5812 ppm respectively, comparable to measured values in other High Ba—Sr granites, both in the Late Caledonian NHG suite (Fowler et al., 2008) and worldwide (e.g. Lara et al., 2017; Tarney and Jones, 1994; Ye et al., 2008). In addition, high Cr (up to 407 ppm) and Ni (up to 433 ppm) contents, across the range of rock types that the Ratagain Complex comprises, indicate mantle derivation and further confirms

Table 1
Representative whole-rock geochemical analyses for the range of rock compositions present in the Ratagain Complex. Key to abbreviations: G is granite; Grd is granodiorite; Md is monzodiorite; Mz is monzonite; Sy is syenite; QzG is quartz-rich granitoid; Qmd is quartz monzodiorite; Qmz is quartz monzonite.

Sample	Sy	Mz			Md		Grd	QrG	G				Qmz			Qmd			
	AL 071	AL 017	AL 059	AL 067	AL 031	AL 062	AL 054	AL 011	AL 013	AL 038	AL 072	AL 100	AL 063	AL 079	AL 081	AL 002	AL 009	AL 045	AL 096
Major oxides (wt%)																			
SiO_2	45.72	56.16	62.77	54.84	64.39	57.00	65.69	81.92	71.88	70.31	65.20	69.74	68.21	65.97	59.87	67.54	67.98	69.75	62.53
TiO_2	1.62	0.68	0.43	1.74	0.39	0.84	0.46	0.37	0.17	0.36	1.25	0.43	0.36	0.49	0.93	0.46	0.40	0.43	0.74
Al_2O_3	11.36	14.05	18.05	11.57	18.27	16.42	17.06	9.04	14.71	15.78	14.23	13.98	15.76	16.22	14.24	16.58	16.70	16.07	15.48
Fe_2O_3	6.88	6.46	2.89	8.42	2.51	5.33	3.29	2.10	0.91	1.86	2.84	2.33	2.21	3.21	5.14	2.75	2.74	1.97	6.23
MnO	0.11	0.10	0.04	0.13	0.03	0.08	0.01	0.03	0.02	0.01	0.11	bdl	0.03	0.04	0.08	0.04	0.04	0.07	bdl
MgO	9.50	3.12	0.59	7.24	0.74	3.69	0.55	0.35	0.22	0.44	1.66	2.56	0.95	1.96	4.11	1.22	1.13	0.29	3.03
CaO	9.74	6.60	1.66	7.95	1.47	4.57	1.20	0.48	0.97	0.70	2.54	1.26	1.77	1.27	4.77	2.10	1.23	1.47	3.74
Na_2O	2.20	3.95	5.52	2.80	6.55	5.60	5.09	2.26	5.22	5.22	2.45	4.26	5.33	4.89	3.75	5.67	5.78	5.82	3.81
K_2O	5.98	5.19	5.25	4.84	4.95	3.48	3.90	2.58	4.60	4.88	4.88	4.83	4.07	5.53	5.29	3.72	4.04	3.93	3.56
P_2O_5	2.47	0.90	0.18	1.52	0.19	0.63	0.27	0.05	0.03	0.18	0.34	0.28	0.18	0.29	0.88	0.22	0.20	0.24	0.33
LOI	0.56	0.37	0.52	0.59	0.44	0.51	1.81	1.00	1.26	0.87	0.96	0.82	0.31	0.71	0.59	0.89	1.35	1.63	0.98
Total	96.14	97.57	97.90	101.65	99.94	98.14	99.32	100.17	99.97	100.62	96.45	100.49	99.18	100.58	99.65	101.19	101.58	101.66	100.43
Trace elements (ppm)																			
Ba	3778	2371	5812	2139	2720	2620	2491	1026	1570	1802	786	1880	2693	1533	1816	1842	1657	1859	1181
Rb	97	91	47	85	39	45	65	47	75	75	98	75	70	59	99	62	68	74	42
Sr	2228	2724	4101	1825	2017	2427	1258	283	610	1337	416	1588	1579	1464	1437	1443	1223	1214	815
Nb	16	21	54	14	11	9	14	6	8	12	12	14	13	15	15	9	12	15	7
Zr	257	301	814	227	236	202	239	146	122	152	310	183	179	196	257	164	194	184	138
Y	32	26	34	28	14	19	19	9	12	13	30	16	14	13	22	14	15	16	14
Th	12	37	45	13	4	5	8	11	13	7	9	11	8	15	22	6	14	12	6
Cr	407	47	37	343	31	163	84	139	71	56	98	40	70	45	193	131	64	112	180
Ni	304	209	131	317	136	193	178	433	292	161	137	114	96	142	277	161	253	103	219
V	160	116	61	116	39	117	59	42	9	51	129	47	45	43	105	55	48	53	105
Cu	23	7	7	1	bdl	35	3	7	14	23	34	7	1	1	bdl	1	1	8	19
Zn	98	68	39	99	33	71	41	bdl	bdl	1	46	39	42	32	71	16	40	17	51
La	97.7	191	87.5	72.9	74.9	65.1	120	35.7	43.7	85.5	42.1	61.3	56.1	63.9	104	51.9	109	85.4	18.6
Ce	196	396	191	148	151	133	259	75.4	85.7	141	86.4	95.8	111	129	203	112	214	147	39.4
Pr	21.7	49.2	23.4	17	16.9	15.1	25.9	7.6	9.1	13.8	10.2	8.8	11.9	12.1	23.1	12.6	24.6	16.2	4.2
Nd	73.6	165.7	86.3	61.9	59.3	56.1	92.8	23.6	28.1	45.9	38.5	28.7	42.1	41.8	84.6	40.8	78.3	55.7	16.5
Sm	12.3	24.3	14.6	10.9	8.1	9.3	14.9	3.3	3.9	5.6	7.1	3.6	6.7	6.7	14.6	5.7	10.8	9	2.9
Eu	3.3	6.4	3.7	2.1	2.5	2.3	4.1	1	1.4	1.5	1.4	0.8	1.8	1.6	3.2	1.8	3.3	2.4	0.7
Tm	bdl	0.39	bdl	bdl	bdl	bdl	bdl	0.06	0.11	bdl	bdl	bdl	bdl	bdl	bdl	0.1	0.18	bdl	bdl
Yb	1.42	2.2	1.36	0.81	0.84	0.70	1.08	0.37	0.69	0.42	3.00	0.50	0.62	0.63	1.16	0.6	1.08	0.86	0.70
Lu	bdl	0.35	bdl	bdl	bdl	bdl	bdl	0.08	0.11	bdl	bdl	bdl	bdl	bdl	bdl	0.09	0.17	bdl	bdl

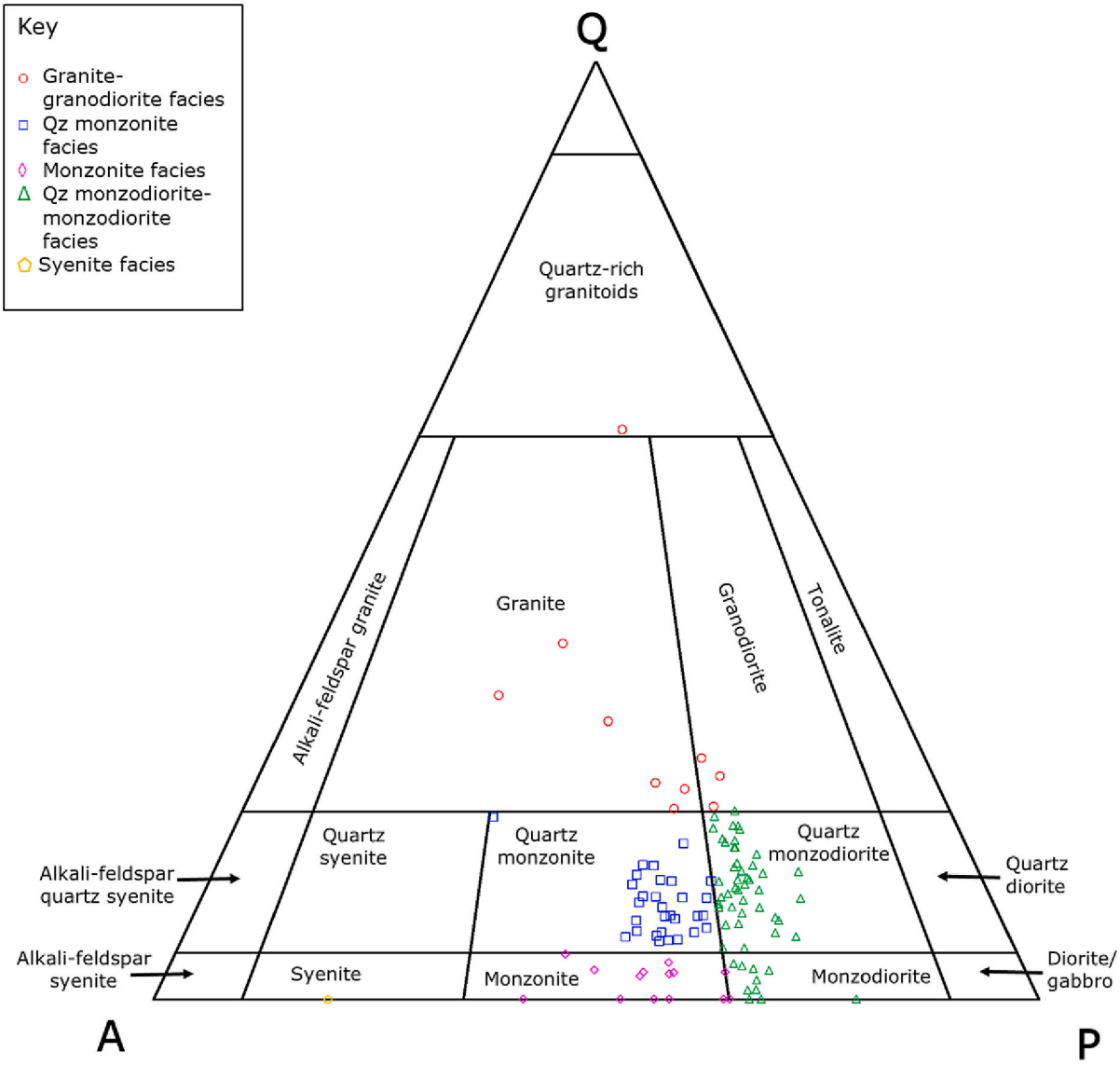

Fig. 3. QAP rock classification diagram (Streckeisen, 1976) showing the rocks of the Ratagain Complex sampled in this study using the CIPW normative mineralogy (Irvine and Baragar, 1971) calculated from lithogeochemical analysis and plotted in TERNPLOT (Marshall, 1996). Key to abbreviations: Q is quartz; A is alkali-feldspar; P is plagioclase.

magma mixing between mantellic mafic and crustal silicic end members (e.g. Fowler et al., 2001, 2008; Fowler and Henney, 1996; Lara et al., 2017; Tarney and Jones, 1994).

Chondrite-normalized diagrams (Sun and McDonough, 1989; Fig. 9A) indicate a depletion of heavy REEs (HREEs) relative to the light REEs (LREEs) in all the studied facies, as HREE concentrations are typically around 10× chondrite values, whilst the LREE concentrations mainly lie between 100 and 1000× chondrite values. There is a conspicuous absence of significant Eu anomalies. The most pronounced depletions occur in the granite-granodiorite facies whilst the quartz monzodiorite-monzodiorite facies and monzonites have less-depleted HREE patterns.

Primitive-mantle-normalized trace-element spider diagrams (McDonough and Sun, 1995; Fig. 9B) show enrichment in large-ion lithophile elements (LILEs) including Rb, Ba, K and Sr, suggesting that feldspar was not a fractionated and/or residual phase.

Notable depletions occur in high field strength elements (HFSEs) including U, Th, Nb, Zr and are particularly pronounced in P and Ti. The deep P and Ti troughs relative to the other HFSE are indicative of selective removal of Ti and P by one or more mineral phases; in the Late Caledonian Rogart and Ach'Uaine intrusives such elemental characteristics have been ascribed to apatite and titanite fractionation (Fowler et al., 2008).

4.3. *Radiogenic isotopes*

New Rb—Sr and Sm—Nd radiogenic isotope data for five samples are presented in Table 2. The isotopic compositions, when recalculated using Rogers and Dunning (1991) crystallisation age of 425 Ma yield a range of $^{87}Sr/^{86}Sri$ values from 0.7056 to 0.7062. $143Nd/144Nd_i$ values fall between 0.511409 and 0.511485 and negative εNd values (ca. − 11.8 to −13.3) point to an enriched source region for the Ratagain Complex. This is confirmed by the εNd vs $^{87}Sr/^{86}Sr_i$ diagram (Fig. 10), which plots the new isotope data alongside published isotope work for the NHG high Ba—Sr suite. The Ratagain samples investigated in this study form an enriched cluster comparable to the syenite-dominated intrusions (e.g. Loch Loyal and the Loch Borralan syenite).

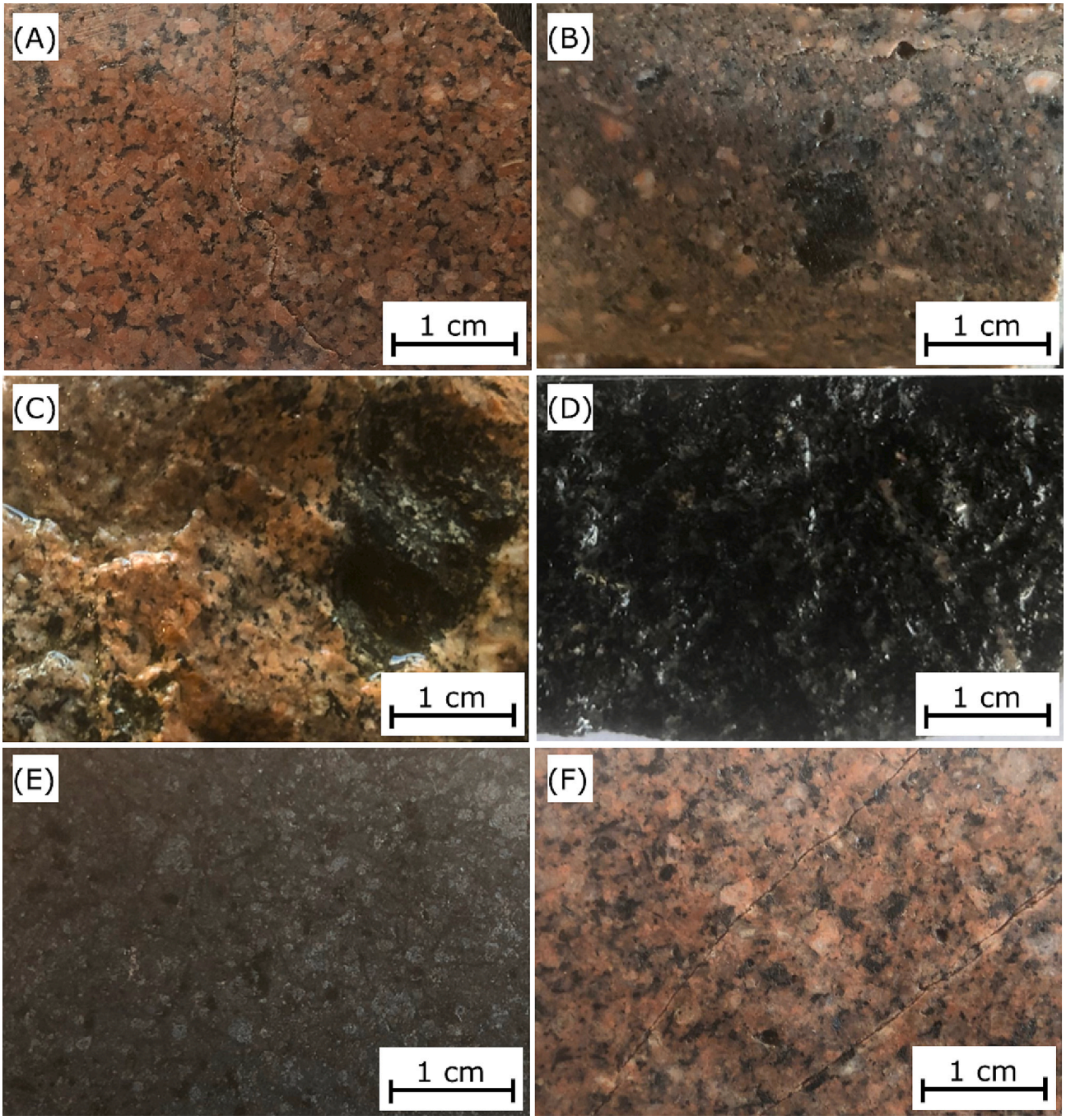

Fig. 4. Representative hand specimen photographs of the various facies of the Ratagain Complex. (A) Quartz monzonite showing a medium-grained porphyritic texture (B) Porphyritic monzodiorite sample in which pinkish alkali feldspar phenocrysts stand out from a dark fine-grained matrix of quartz, plagioclase feldspar and biotite (C) Medium-grained granite hosting a dark mafic microgranular enclave (D) Close view of a large mafic microgranular enclave (E) Medium-grained granodiorite (F) Monzonite sample with a coarse-grained porphyritic texture.

5. Discussion

5.1. Implications for the Late Caledonian granite suite

The major element data presented above from the Ratagain Complex overlap with the entire compositional range of the Northern Highlands high Ba—Sr suite (Fowler et al., 2008). In terms of trace elements, the rocks closely resemble the mingled and mixed appinites at Ach'Uaine ca. 100 km to the NE. Further, the field observations and rock magnetic data of Lawrence et al. (2022) evidence that the Ratagain Complex bears a primary (i.e. magmatic) magnetic fabric with a subtle tectonic overprint imparted by sinistral transpressive strain. Critically, this overprint did not develop into a full tectonic fabric (Lawrence et al., 2022). The authors interpreted this magnetic fabric as being formed post-emplacement when the granite was near solidus temperature and in a crystal-rich but magmatic state. Taken in context with previous radiometric ages for the intrusion (Rogers and Dunning, 1991; Thirlwall, 1988; Turnell, 1985) and knowledge of the timing of Acadian regional deformation (Miles et al., 2016; Woodcock et al., 2019) the magnetic characteristics of Ratagain suggest that the complex is either younger than the reported 425 ± 3 Ma age (Rogers and Dunning, 1991) and records later Acadian transpression (see Mendum, 2012; Miles and

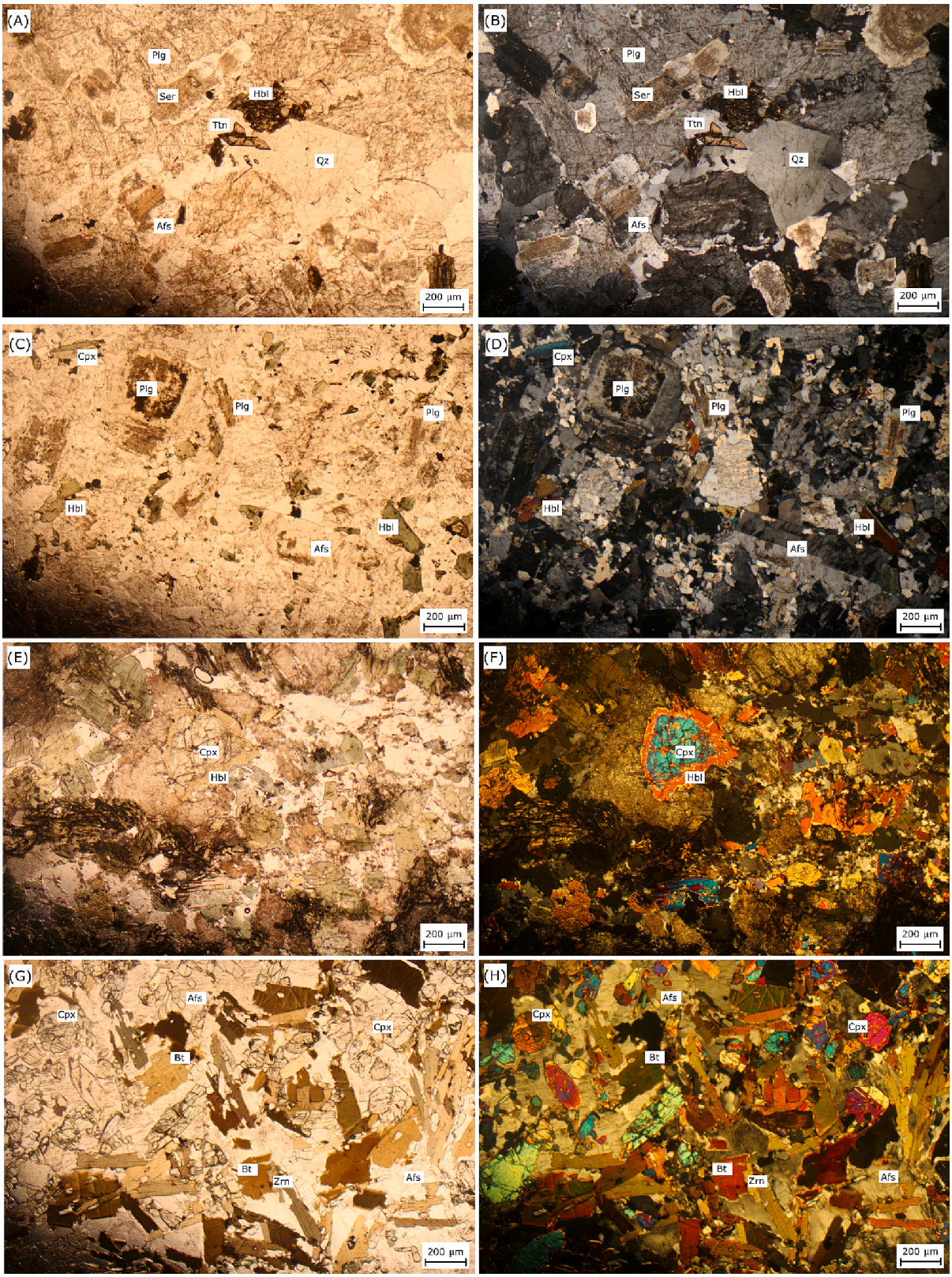

Fig. 5. Representative photomicrographs of the various facies of the Ratagain Complex (A) PPL image of granodiorite with euhedral titanite and hornblende set in a groundmass of quartz, alkali feldspar and sericitized plagioclase (B) XPL image of granodiorite (C) PPL image of quartz monzonite showing plagioclase phenocrysts with relict compositional zoning, alkali feldspar with simple twinning and minor hornblende and clinopyroxene (D) XPL image of quartz monzonite (E) PPL image of quartz monzodiorite with large, equidimensional clinopyroxene crystals surrounded by a hornblende alteration rim (F) XPL image of quartz monzodiorite (G) PPL image of syenite consisting of abundant ferromagnesian phases, including twinned clinopyroxene and biotite with pleochroic haloes around enclosed zircon (H) XPL image of syenite. Mineral abbreviations after Whitney and Evans (2010).

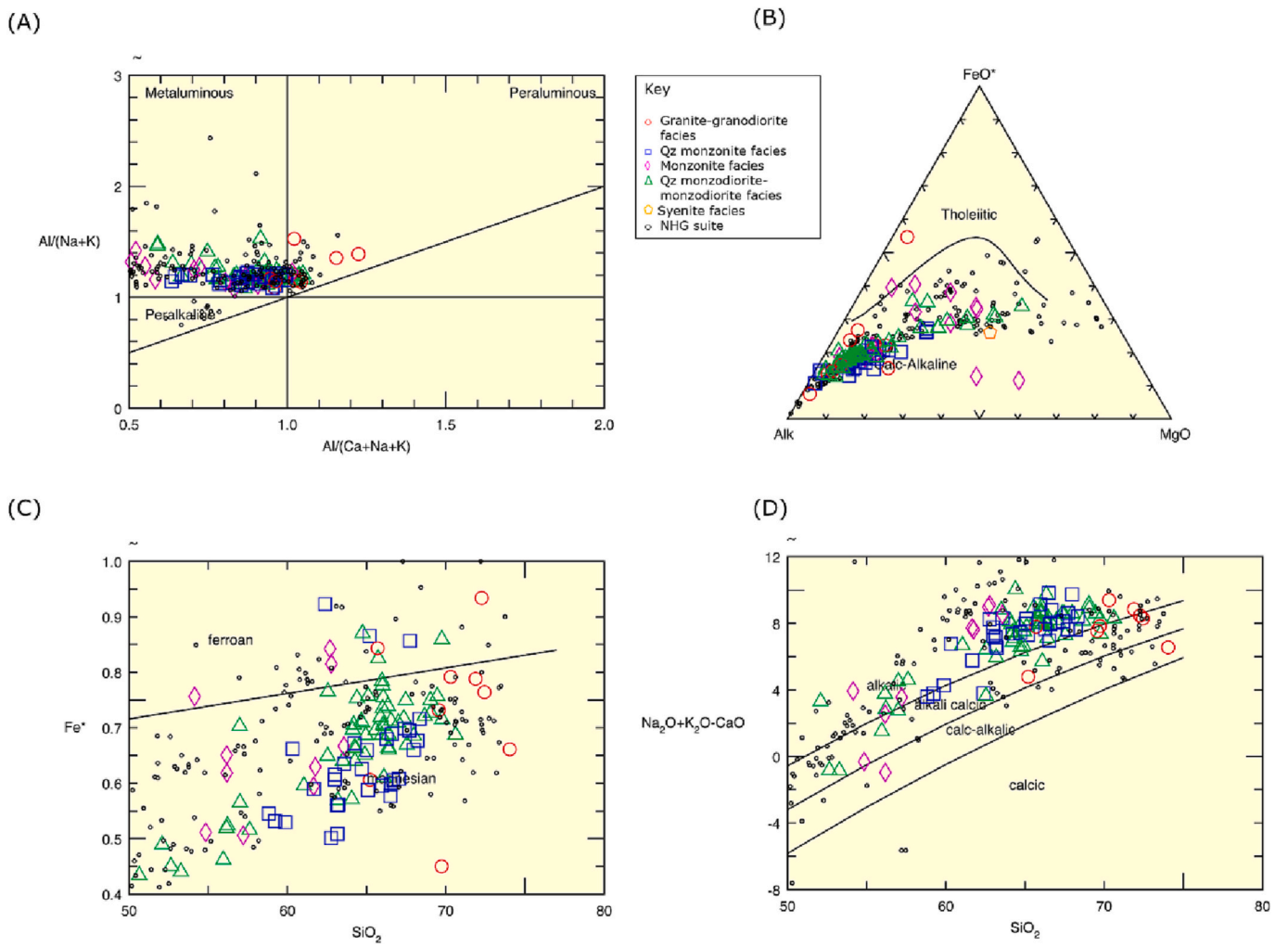

Fig. 6. Geochemical characteristics of the various facies in the Ratagain Complex. Also plotted are data from Thompson and Fowler, 1986, Thirlwall and Burnard, 1990, Fowler, 1992, Fowler and Henney (1996), Fowler et al. (2001, 2008). Coloured symbols are data from this investigation and open black circles are compiled literature data for the Northern Highland Granite Suite (NHG). (A) Alumina Saturation index diagram after Maniar and Piccoli (1989); (B) AFM diagram of Irvine and Baragar (1971); (C)FeOt/ (FeOt+ MgO) versus SiO2 diagram; fields of ferroan and magnesian series from Frost et al. (2001); (D) Modified Alkali Lime Index diagram of Frost et al. (2001).

Woodcock, 2018; Woodcock et al., 2019), or that it was intruded and emplaced incrementally over a protracted time period, whereby incremental remobilisation by successive magma pulses accommodated most of the ambient tectonic strain, enabling the preservation of the primary magmatic fabric whilst simultaneously preventing the full development of a solid-state tectonic fabric.

Thus, the Ratagain Complex's petrogenesis and emplacement are consistent with transcrustal crystal mush models that have advanced granite emplacement and magma evolution understanding in recent years (Cashman et al., 2017; Jackson et al., 2018; Sparks et al., 2019). This is more likely to occur at mid-crustal levels wherein the accreting intrusion was remobilized periodically by succeeding replenishments of magma, with exchange of crystals and melt between resident material and each successive magmatic pulse resulting in highly diffuse or indistinguishable internal contacts (Miller et al., 2011).

The emplacement of new magma pulses into partially-crystallised magma mush at mid-crustal depths could also have accommodated most of the strain and temperature increase (Lui et al., 2018) and offers a plausible explanation as to why the Ratagain Complex bears no obvious solid-state fabric (Lawrence et al., 2022), contacts the host Precambrian rock without a thermal aureole (Fig. 3A, E,) and carries isotopic signatures consistent with a lower-crustal Lewisian granulite contaminant as well as the overlying Moine rocks (Fig. 10).

In addition to the Ratagain Complex, other Caledonian granites show evidence for long-lived, pulsatory magmatism. *Re*-examination of the emplacement history of the Shap granite, Lake District through high-precision U—Pb zircon dating, suggests a protracted history of magmatic activity in the order of 106 Ma and zircon crystallisation at deep crustal levels in a crystal-mush system (Miles and Woodcock, 2018). The Shap granite also offer evidence of repeated rejuvenation of this crystal mush in its field features ranging from macroscopic enclaves to microscopic complex zoning patterns in magmatic alkali-feldspar phenocrysts, the former representing voluminous magmatic pulses and the later resulting from smaller magmatic injections (Miles and Woodcock, 2018).

Further, parallels can also be drawn with the Donegal Batholith, Ireland, which has a similar compositional variation and magmatic evolution to the Ratagain Complex (Archibald and Murphy, 2021). Of note here is that the Donegal Batholith is composed of a number of discrete intrusive bodies, each recording pulsed emplacement. Each intrusion is quite homogeneous, especially the younger ones, and all the intrusions were emplaced rapidly over a period of ca. 30 Myr (Archibald and Murphy, 2021). The exception is the highly heterogeneous Main Donegal Granite, which contains units that seem to represent each of the surrounding intrusions and its emplacement spans the time frame of the other intrusions (Stevenson et al. 2008). Stevenson et al. (2008)

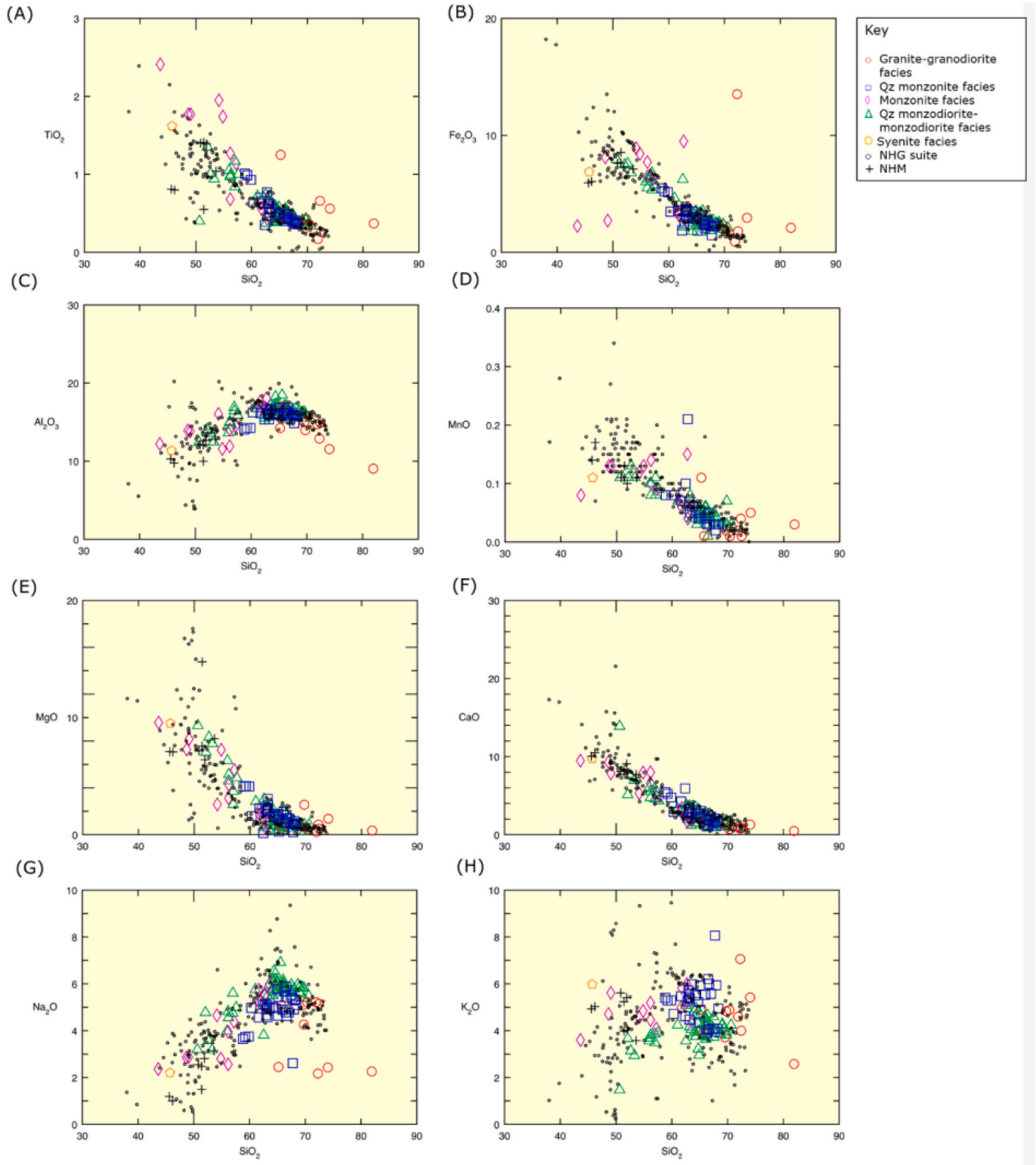

Fig. 7. Variation diagrams for major element oxides (in weight %) plotted against SiO_2 for the Ratagain Complex and NHG suite. Also included for comparison are data for Northern Highland minettes (NHM) (Canning et al., 1996).

developed a model where the Main Donegal Granite represents the long lived and deeply penetrating feeder zone for the surrounding satellite plutons in the upper crust. Although the Ratagain Complex does not have a suite of satellite plutons, we draw the comparison of a mid-crustal feeder zone and propose that the intrusive body existed as a part of a vertically-linked sheeted-system potentially controlled by sinistral shearing (Lawrence et al., 2022).

We therefore suggest that many Caledonian granites previously interpreted as rapidly-emplaced, shallow-crustal intrusions (e.g. Watson, 1984) actually represent more long-lived, mid-crustal intrusions and that the large, euhedral zircons selected for analysis in the older geochronology studies (e.g. Rogers and Dunning, 1991) represent grains

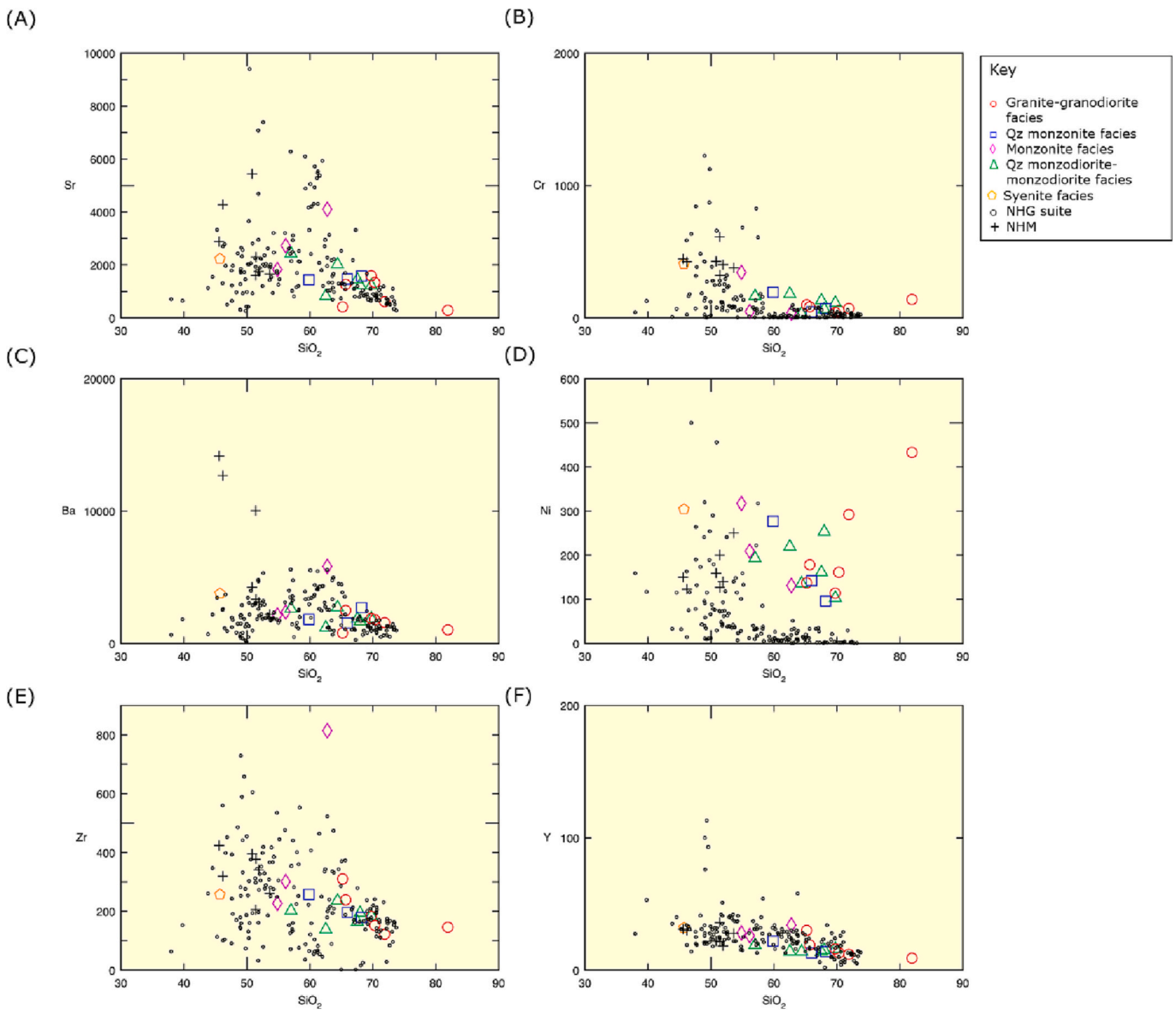

Fig. 8. Variation diagrams for selected trace elements (in ppm) plotted against SiO_2 for the Ratagain Complex, NHM and NHG suite.

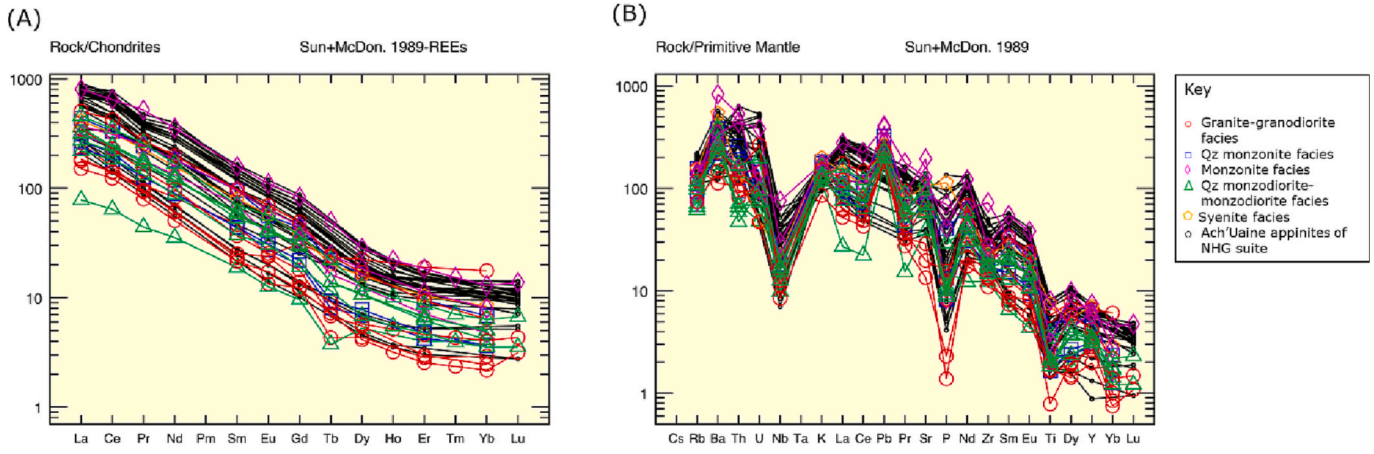

Fig. 9. (A) Chondrite-normalized REE diagrams and (B) primitive-mantle-normalized trace-element spider diagrams for samples from the Ratagain Complex. Open black circles are literature data for the Ach'Uaine appinites of the NHG suite. Normalizing values are from Sun and McDonough (1989) and McDonough and Sun (1995).

Table 2
Representative whole-rock radiogenic isotope data for samples from the Ratagain Complex. Key to abbreviations: G is granite; Mz is monzonite; Qmz is quartz monzonite. *U-Pb baddeleyite age after Rogers and Dunning (1991)- see discussion for limitations of older geochronology studies.

Sample	Facies	Sr	Rb	$^{87}Sr/^{86}Sr$	$^{87}Sr/^{86}Sr_i$	Sm	Nd	$^{143}Nd/^{144}Nd$	$^{143}Nd/^{144}Nd_i$	εNd(t)	t(Ma)*
AL013	G	589	54.7	0.707413	0.705784	2.88	23.2	0.511618	0.511409	−13.3	425
AL059	Mz	7014	57.7	0.706021	0.705789	35.9	203	0.511782	0.511485	−11.8	425
AL063	Qmz	1613	50.9	0.706068	0.705515	5.96	41.5	0.511651	0.511410	−13.3	425
AL074	G	2844	53.5	0.706516	0.706187	13.6	87.6	0.511679	0.511418	−13.1	425
AL092	G	1980	53.4	0.706231	0.705759	7.23	49.3	0.511658	0.511420	−13.1	425

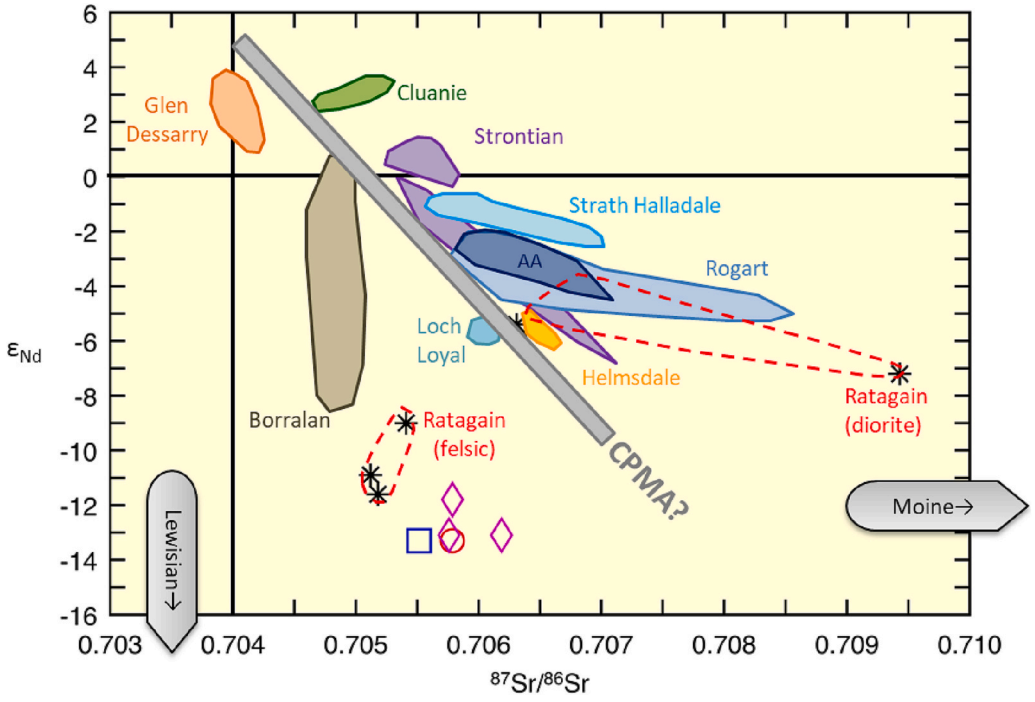

Fig. 10. Initial Nd vs initial Sr isotope plot for selected samples from the Ratagain Complex. Also plotted are selected samples from the NHG suite including the Ach'Uaine Appinites (AA), Borralan, Cluanie, Glen Dessary, Helmsdale, Loch Loyal, Strath Halladale, Strontian and Rogart (Fowler et al., 2008) and the hypothetical Caledonian Parental Magma Array (CPMA).

formed in the deep crust, early in the magmatic history. Thus whilst the early U—Pb zircon ages need not be discounted, they can be viewed as maxima for the timing of granite emplacement. Our interpretation is consistent with the large spread of crystallisation ages between c.435–390 Ma (Soper, 1986) for the Caledonian intrusives and could also account for the extended magmatism after active Iapetan subduction and slab failure.

5.2. *Slab-failure versus arc nature of the rocks*

Petrogenetic models for high Ba—Sr magmas fall largely into two camps for the Caledonian examples and worldwide. The first (e.g. Fowler et al., 2008, Bao et al., 2019) holds that compositional continuity between felsic and mafic members of the suite require a genetic relationship and that a significant component of the granite magmatism is ultimately juvenile. The second (e.g. Neilson et al., 2009; Ye et al., 2008) argues that the mafic components are mantle-derived but that the granites represent crustal melts which subsequently interact with the contemporaneous mafic magmas. This model requires no genetic relationship, no juvenile input to the felsic magmas and fundamentally different sources for the mafic and felsic extremes. However, both hypotheses for the Caledonian examples are consistent with slab failure being responsible for the magmatism, a tectonic setting which is also commonly proposed for similar magmas elsewhere (Leite et al., 2021; Ye et al., 2008). The latter arguments have been considerably strengthened recently, with a regional study of Caledonian magmas (Archibald et al., 2022) in the light of the slab failure tectonomagmatic discrimination diagrams of Hildebrand and Whalen (2017) and Whalen and Hildebrand (2019).

All felsic samples from the Ratagain Complex with SiO_2 concentrations between 55 and 70 wt% and an alumina saturation index (ASI) of <1.1 fall within the slab failure field on the tectonomagmatic discrimination diagrams of Hildebrand and Whalen (2017) and Whalen and Hildebrand (2019), showing high Nb/Y and La/Yb vs. Gd/Yb (Fig. 11A, B) and La/Sm vs. Sm/Yb (Fig. 11C) ratios. On the Nb vs. Y plot (Fig. 11D) two monzonite samples display A-type affinities and two samples of the granite-granodiorite and quartz monzodiorite facies respectively plot within the arc field. This could be accounted for by the alteration of Rb-bearing mineral phases such as alkali feldspar, which shows varying degrees of sericitization in all samples (Fig. 5A–D).

Nearly all of the Ratagain samples exhibit slab-failure signatures according to the Rb vs. Ta + Yb diagram (Fig. 12B) and La/Yb vs. Sr/Y plot (Fig. 12D) The Rb vs. Nb + Y (Fig. 12A) and Nb/Yb vs. Sr/Y (Fig. 12C) show more scatter; as before, this can be accounted for by the mobility of Sr and Rb and related feldspar alteration.

Therefore, the following discussion assesses the new data from Ratagain in the context of slab failure and highlights new constraints and insights from this unique Caledonian intrusion.

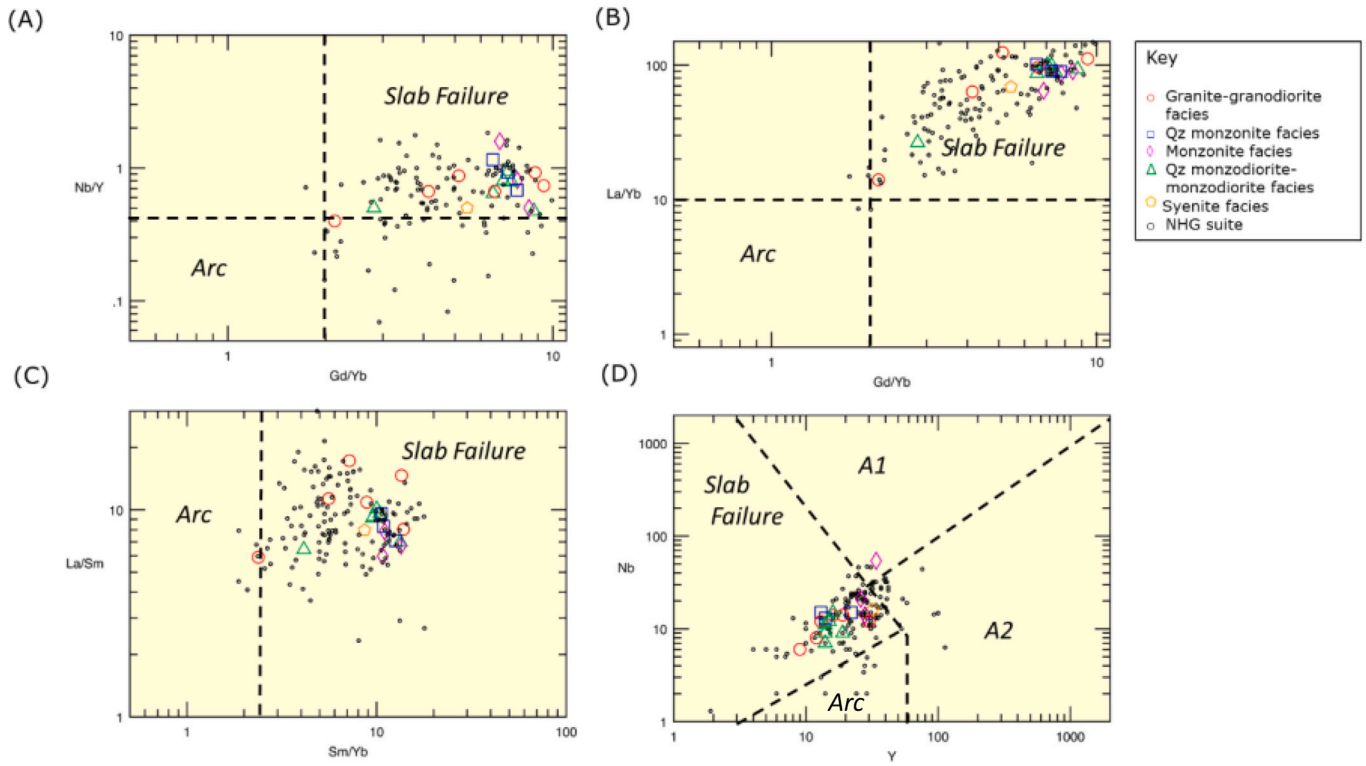

Fig. 11. Tectonomagmatic discrimination diagrams showing slab-failure, arc and A-type fields (Hildebrand and Whalen, 2017; Whalen and Hildebrand, 2019) for samples from the Ratagain Complex with 55 to 70 wt% SiO2 and an ASI value of 1.1 or less. Open black circles are NHG data. (A) Nb/Y vs. Gd/Yb plot (B) La/Yb vs. Gd/Yb (C) La/Sm vs. Sm/Yb. A1 and A2 fields for A-type granites are after Eby (1992). (D) Nb vs. Y.

5.3. Constraints on magmatic sources and evolution

One of the most noticeable aspects of the Ratagain Complex is the relative abundance of exposed intermediate and mafic rocks (Fig. 2), which are generally subordinate in other members of the Northern Highland high Ba—Sr suite. Fowler et al. (2008) argue that equivalent mafic rocks are likely to be mantle-derived, and so offer information on the SCLM reservoir(s) from which they originated, while Neilson et al. (2009) suggest that the intermediate rocks are derived by "partial melting of heterogeneous mafic to intermediate lowermost crust that had high Ba–Sr derived from previous melting of large ion lithophile element (LILE)-enriched mantle". Assuming that extensive melting of mafic-intermediate rocks is required to derive mafic-intermediate rocks, the only substantive difference is the number of melting events, one in the former hypothesis and two in the latter. In both hypotheses the origin of the distinctive chemistry lies in the SCLM. It should also be noted that Thirlwall (1981, 1982) regards the Lorne high Cr—Ni andesitic (thence intermediate) lavas to be mantle-derived, little modified from primary melt compositions (cf. Neilson et al., 2009). Similarly, calc-alkaline lamprophyres (minettes) from the Northern Highlands (Canning et al., 1996) are thought to represent primary mantle melts and overlap considerably with the more mafic Ratagain samples, as do the monzogabbros and monzodiorites of the Ach'Uaine appinite suite (Fowler, 1988; Fowler and Henney, 1996) which are regarded as hypabyssal equivalents of the lamprophyres (Figs. 7–9).

Given that these are plutonic rocks, the major element variations between the intermediate and felsic rocks can likely be attributed, at least partly, to crystal-liquid equilibration and variable, incomplete mineral separation. Simple least-squares calculations demonstrate residual differences for example evolutionary models, from monzonite to quartz monzonite by separation of amphibole and plagioclase plus biotite or pyroxene, and from monzonite or quartz monzonite to granite by separation of K-feldspar, plagioclase and amphibole (Table 3). This is consistent with the observed petrography (Figs. 4–5). Principal component analysis (PCA) conducted on the major element oxides results in ten principal components (see Supplementary Table SC2); the first principal component (PC1) accounts for 66.7% of the overall variance, the second principal component (PC2) accounts for 12.9% of the overall variance and the third principal component (PC3) accounts for 9.6% of the overall variance. Accordingly, the first three out of the ten principal components are responsible for 90% of the overall variation of the major element oxides and only the first two components have eigenvalues >1 (and ~ 80% of the overall variance). Heavily loaded on PC1 are silica (negative) and all the mafic mineral components (MgO, Fe_2O_3, MnO, CaO: all positive). TiO_2 (titanite) and P_2O_5 (apatite) are also both positively loaded onto PC1. PC2 separates the felsic components, Na_2O and Al_2O_3 (negative) with K_2O positive. The associated scores plot (Fig. 13) separates monzodiorites and monzonites along the mafic vectors, quartz monzonites broadly around the origin (quartz monzonite dominates the sample set) and granites along the K_2O vector on PC2. Importantly, there is a continuum between the different samples, from most mafic to most felsic. Thus, this objective statistical technique is also consistent with variable mineral separation within genetically-related evolving magmas.

Previous isotopic evidence (Fowler et al., 2008) suggests concurrent crustal contamination affected the NHG, but to an extent that does not obscure the enriched mantle origin if the elemental coherence of the suite is accepted as evidence of a genetic relationship. Our new isotope data indicates that the generation of the Ratagain magmas did involve recycling of ancient continental crust. The Nd—Sr isotope covariations for our studied samples (Fig. 10) diverge from the fractionation pathways of the other calc-alkaline granites, including previously-sampled "diorites" from the Ratagain Complex that trend towards the local Moine metasediments (Fowler et al., 2008). Our samples instead plot similar trajectories to the NHG syenites, exhibiting $^{87}Sr/^{86}Sr_i$ values and very low εNd values (ca. −11.8 to −13.3) that are likely the result of

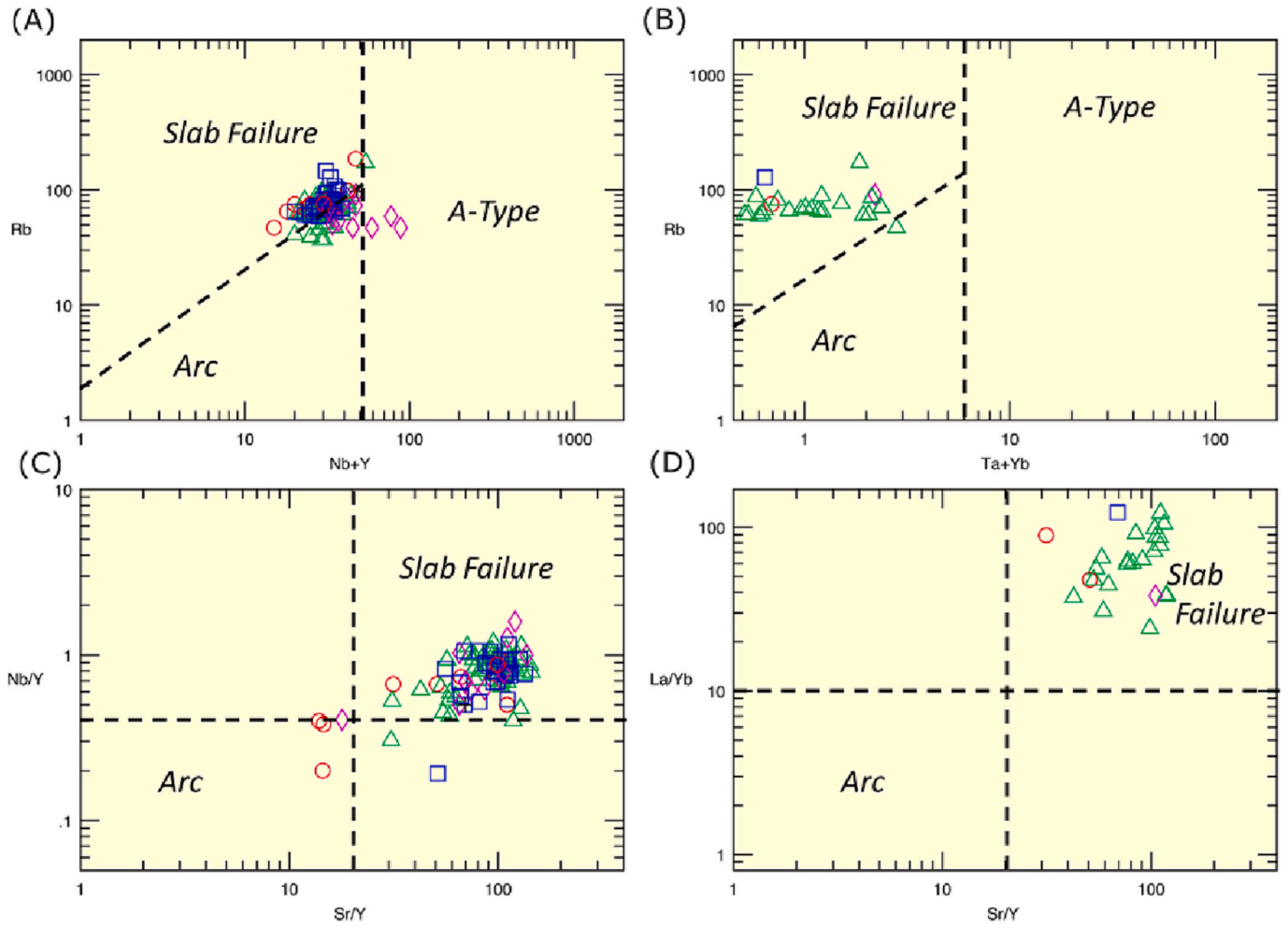

Fig. 12. Tectonomagmatic discrimination diagrams (Hildebrand and Whalen, 2017; Whalen and Hildebrand, 2019) plotting samples from the Ratagain Complex with a SiO_2 concentration between 55 and 70 wt% and ASI of <1.1. Also shown for comparison are the NHG data. (A) Rb vs. Nb + Y (B) Rb vs. Ta + Yb (C) Nb/Sr vs. Sr/Y (D) La/Yb vs. Sr/Y.

Table 3
Summary least-squares mixing models of crystal fractionation in the Ratagain Complex.

Fractionation step	Samples	Major fractionating minerals	Sum r^2
Monzonite to monzonite	AL092 - AL059	Amphibole, plagioclase, pyroxene	2.48
Monzonite to quartz monzonite	AL092 – AL063	Amphibole, plagioclase, biotite	3.05
Monzonite to granite	AL059 – AL013	Alkali feldspar, plagioclase, amphibole	0.17
Monzonite to granite	AL059 - AL703	Alkali feldspar, plagioclase, amphibole	0.23
Quartz monzonite to granite	AL063 – AL013	Alkali feldspar, plagioclase, amphibole	1.57
Quartz monzonite to granite	AL063 – AL073	Alkali feldspar, plagioclase, amphibole	1.84

contamination with Rb-depleted Lewisian granulite facies rocks. This suggests significant incorporation of Archean-Paleoproterozoic Lewisian granulite at lower crustal depths as opposed to in-situ contamination in upper crustal magma chambers by Neoproterozoic Moine rocks (Fowler et al., 2008).

5.4. Implications for slab failure magmatism and granite petrogenesis

The Ratagain intrusion and other members of the Northern Highland high Ba—Sr suite plot firmly in the slab failure fields on the appropriate tectonomagmatic discrimination diagrams (Figs. 11–12) and indeed have been interpreted previously as the magmatic consequence of slab break-off (Atherton and Ghani, 2002; Fowler et al., 2008; Miles et al., 2016; Neilson et al., 2009). This is essentially a result of their characteristic enrichment in LILEs and depletion in HFSEs, generating high Sr/Y and La/Yb ratios. Such ratios and associated characteristics are normally ascribed to melting processes involving garnet and/or amphibole stability in the residue, effectively withholding HREEs and associated elements from any equilibrated melt. These are amongst the definitive characteristics of adakitic rocks derived from intra-crustal melting of basalts, and Whalen and Hildebrand (2019) attribute them similarly to ocean crust melting during slab failure at mantle depths. However, there is an alternative to garnet/amphibole residual control that is capable of generating the same characteristic element ratios - extreme enrichment in LILEs without active “depletion” in HFSEs. The characteristic REE pattern of adakite (and TTG which are widely agreed to have been generated by basalt melting) has high LREE and low to very low HREE (<<10× chondrites). The Ratagain Complex (and other Northern Highland high Ba—Sr intrusions) have Yb values that range either side of 10 and up to ca. 20, are extremely enriched in LREE (Ce commonly several hundred and up to 1000× chondrites). Total REE concentrations

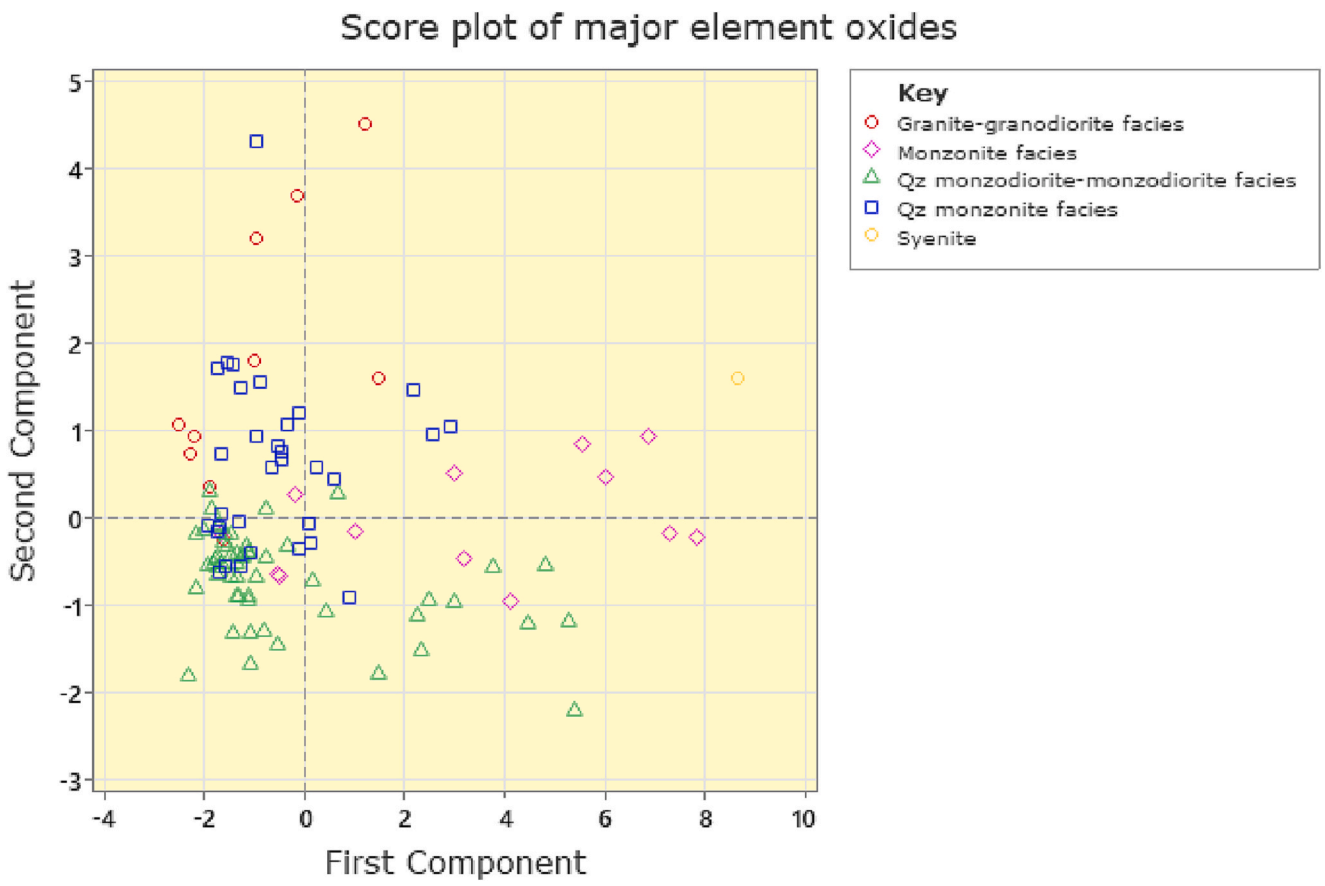

Fig. 13. Principal component analysis (PCA) biplot of PC1 vs. PC2 scores for samples from the Ratagain Complex.

start high and ultimately decrease with silica concentration, generating genuinely-depleted HREE only as a result of crystal fractionation removal of observed and abundant amphibole, titanite, apatite and zircon. Importantly, the mafic rocks also carry the isotopic signature of extreme LILE enrichment and $^{87}Sr/^{86}Sr$ up to 0.7062 and εNd as low as −13.3. If the slab failure signature were in this case generated by garnet/amphibole in the residue of ocean crust melting, the isotopic character should reflect long-term incompatible element depletion. The simplest explanation is that slab melting also affected the subducted sediment carapace, which infused the overlying SCLM with (possibly additional) enrichment, before being fused by the thermal anomaly resulting from asthenosphere encroachment (Fowler et al., 2008). The elemental and isotopic similarity between the slab failure magmas and broadly coeval lamprophyres, which are generally considered to be primary melts from the SCLM, supports this interpretation.

The felsic rocks of the Ratagain intrusion exhibit such strong elemental similarities to those of the mafic-intermediate rocks that a fundamentally different source is unlikely. Furthermore, any source within the stability range of plagioclase would not generate very high Sr in equilibrated magmas, and would produce negative Eu anomalies - which are conspicuous by their absence here (but are otherwise very common in "I-type" granites). Thus, the felsic rocks represent fractionated versions of "post-collisional mafic magmas", whose origin has been linked to unrecognised crustal growth since the Archaean (Couzinié et al., 2016). Such magmas have zircon Hf—O compositions appropriate to crustal derivation (i.e. negative εHf associated with elevated δ18O), but are dominated in terms of bulk mass by the mantle component (62–85%, Couzinié et al., 2016). The whole-rock Nd and O isotope compositions of Northern Highland high Ba—Sr felsic magmas are reflected in equivalent Hf—O systematics in zircons (Bruand et al., 2019). It therefore seems important to constrain the crust vs. mantle proportions in the high Ba—Sr microcosm that is the Ratagain intrusion (cf. Jacob et al., 2021; Moyen et al., 2021). Outline calculations in Fowler et al. (2008) constrained an average source sedimentary contribution to less than ca. 10% and a crustal contamination contribution via AFC to less than ca. 20%. A combination of both maxima gives a broadly similar estimate to the more rigorous result of Couzinié et al. (2016). As discussed above, the Nd and Sr isotope data included in Fowler et al. (2008) combined with those presented in this study, show that whilst some diorites from the Ratagain Complex define a trend from an enriched mantle source towards the local Moine metasediments, others and the more "felsic" compositions are consistent with contamination with Lewisian granulite, from a similar point on the "Caledonian Parental Magma Array" (CPMA). The Ratagain source composition on that array is towards the enriched end (though not quite the extreme represented by Loch Loyal syenites and the Helmsdale granite) and is consistent with 5–10% sediment contribution, with a variable local crustal component of a few tens percent in the exposed rocks, but around 30% at maximum.

6. Conclusions

Our new lithogeochemical data for the Ratagain Complex, NW Scotland, indicate that it is a high Ba—Sr, slab-failure intrusion and thus support regional geological syntheses invoking slab-failure origin for the Northern Highland high Ba—Sr and wider Late Caledonian intrusive suites.

The major element data presented in this study overlap with the entire compositional range of the Northern Highlands high Ba—Sr suite, and the Ratagain intrusion is transitional between the granites and syenites of the Northern Highlands Terrane.

The $^{87}Sr/^{86}Sr$ values (0.7055 to 0.7062) and low initial εNd values

(− 11.8 to −13.3) indicate that contamination by Lewisian continental crust was volumetrically more significant than evident in previous studies.

The geochemical characteristics may be attributable to a long-lived, incremental emplacement of the complex with crystallisation of successive magma batches originating from the same Caledonian Parental Magma Array but differing in age and extent of assimilation-fractionation.

We therefore propose that literature dates for the Late Caledonian intrusions, particularly those obtained from older geochronology studies, may record crystallisation in the deep crust and not be a valid proxy for granite emplacement. There is thus a need for careful review of previous dates for the Late Caledonian intrusions, to better resolve the links between their petrogenesis, crustal tectonics, the geodynamics of Iapetus subduction, collision and slab break-off.

Declaration of Competing Interest

The authors declare that they have no known competing financial interests or personal relationships that could have appeared to influence the work reported in this paper.

Acknowledgements

AL thanks the Open University, Edinburgh Geological Society and Geologists' Association for the award of the Ian Gass Bursary, Fieldwork Grant and New Researcher's Award, respectively, to conduct field work in the Scottish Highlands. AL also thanks parent carers Paul and Manpreet Lawrence for facilitating fieldwork in the remote Scottish Highlands- no small undertaking!

The assistance provided by Zoe Whittaker in XRF and LAICPMS sample preparation and analysis is gratefully acknowledged.

References

Alderton, D.H.M., 1988. Ag-Au-Te mineralisation in the Ratagain complex, northwest Scotland. Trans. Inst. Mining Metal. (Sect. B App. Earth Sci.) 97, B171–B180.

Archibald, D.B., Murphy, J.B., 2021. A slab failure origin for the Donegal composite batholith, Ireland as indicated by trace-element geochemistry. Geol. Soc. Lond. Spec. Publ. 503, 347–370. Available from: https://doi.org/10.1144/SP503-2020-6.

Archibald, D.B., Murphy, J.B., Fowler, M., Strachan, R.A., Hildebrand, R.S., 2022. Testing petrogenetic models for contemporaneous mafic and felsic to intermediate magmatism within the —Newer Granite‖ suite of the Scottish and Irish Caledonides. In: Kuiper, Y.D., Murphy, J.B., Nance, R.D., Strachan, R.A., Thompson, M.D. (Eds.), New Developments in the Appalachian-Caledonian- Variscan Orogen, Geological Society of America Special Paper 554. https://doi.org/10.1130/2021.2554(15) (p. 1–XXX). Available from.

Atherton, M.P., Ghani, A.A., 2002. Slab breakoff: a model for Caledonian, late Granite syn-collisional magmatism in the orthotectonic (metamorphic) zone of Scotland and Donegal, Ireland. Lithos 62, 65–85. Available from: https://doi.org/10.1016/S0024-4937(02)00111-1.

Bao, Z., Xiong, M., Li, Q., 2019. Petrogenesis of late Mesozoic high-Ba–Sr granites in the Qiushuwan CuMo orefield: implications for the distribution of porphyry Mo mineralization in the East Qinling area of Central China. Lithos 348, 105172.

Brown, P.E., Ryan, P.D., Soper, N.J., Woodcock, N.H., 2008. The Newer Granite problem revisited: a transtensional origin for the early Devonian Trans-Suture Suite. Geol. Mag. 145, 235–256. Available from: https://doi.org/10.1017/S0016756807004219.

Bruand, E., Storey, C., Fowler, M., 2014. Accessory mineral chemistry of high Ba-Sr granites from Northern Scotland: constraints on petrogenesis and records of whole-rock Signature. J. Petrol. 55 (8), 1619–1651. Available from: https://doi.org/10.1093/petrology/egu037.

Bruand, E., Storey, C., Fowler, M., Heilimo, E., 2019. Oxygen isotopes in titanite and apatite, and their potential for crustal evolution research. Geochim. Cosmochim. Acta 255, 144–162. Available from: https://doi.org/10.1016/j.gca.2019.04.002.

Canning, J., Henney, P., Morrison, M., Gaskarth, J., 1996. Geochemistry of late Caledonian minettes from Northern Britain: implications for the Caledonian sub-continental lithospheric mantle. Mineral. Magaz. 60 (398), 221–236. Available from: https://doi.org/10.1180/minmag.1996.060.398.15.

Cashman, K.V., Sparks, R.S.J., Blundy, J.D., 2017. Vertically extensive and unstable magmatic systems: a unified view of igneous processes. Science 355 (6331). https://doi.org/10.1126/science.aag3055. Available from.

Couzinié, S., Laurent, O., Moyen, J.F., Zeh, A., Bouilhol, P., Villaros, A., 2016. Post-collisional magmatism: crustal growth not identified by zircon Hf–O isotopes. Earth Planet. Sci. Lett. 456, 182–195. Available from: https://doi.org/10.1016/j.epsl.2016.09.033.

De Paolo, D.J., 1988. Neodymium Isotope Geochemistry. Springer-Verlag, Berlin.

Dewey, J.F., Dalziel, I.W.D., Reavy, R.J., Strachan, R.A., 2015. The Neoproterozoic to Mid-Devonian evolution of Scotland: a review and unresolved issues. Scot. J. Geol. 51 (1), 5–30. Available from: https://doi.org/10.1144/sjg2014-007.

Eby, G.N., 1992. Chemical subdivision of the A-type granitoids: petrogenetic and tectonic implications. Geology 20 (7), 641–644. Available from: 10.1130/0091-7613(1992)020<0641:CSOTAT>2.3.CO;2.

Fowler, M.B., 1988. Ach'uaine hybrid appinite pipes: evidence for mantle-derived shoshonitic parent magmas in Caledonian granite genesis. Geology 16 (11), 1026–1030. https://doi.org/10.1130/0091-7613(1988)016<1026:AUHAPE>2.3.CO;2.

Fowler, M.B., 1992. Elemental and O-Sr-Nd isotope geochemistry of the Glen Dessarry syenite, NW Scotland. J. Geol. Soc. London 149 (2), 209–220.

Fowler, M.B., Henney, P.J., 1996. Mixed Caledonian appinite magmas: implications for lamprophyre fractionation and high Ba-Sr granite genesis. Contrib. Mineral. Petrol. 126 (1), 199–215. Available from: https://doi.org/10.1007/s004100050244.

Fowler, M., Rollinson, H., 2012. Phanerozoic sanukitoids from Caledonian Scotland: implications for Archean subduction. Geology 40, 1079–1082. Available from: https://doi.org/10.1130/G33371.1.

Fowler, M., Henney, P., Darbyshire, D., Greenwood, P., 2001. Petrogenesis of high Ba–Sr granites: the Rogart pluton, Sutherland. J. Geol. Soc. Lond. 158 (3), 521–534. Available from: https://doi.org/10.1144/jgs.158.3.521.

Fowler, M.B., Kocks, H., Darbyshire, D.P.F., Greenwood, P.B., 2008. Petrogenesis of high Ba-Sr plutons from the Northern Highlands Terrane of the British Caledonian Province. Lithos 105, 129–148. Available from: https://doi.org/10.1016/j.lithos.2008.03.003.

Frost, B.R., Barnes, C.G., Collins, W.J., Arculus, R.J., Ellis, D.J., Frost, C.D., 2001. A geochemical classification for granitic rocks. J. Petrol. 42 (11), 2033–2048. Available from: https://doi.org/10.1093/petrology/42.11.2033.

Goodenough, K., Millar, I., Strachan, R., Krabbendam, M., Evans, J., 2011. Timing of regional deformation and development of the Moine Thrust Zone in the Scottish Caledonides: constraints from the U–Pb geochronology of alkaline intrusions. J. Geol. Soc. Lond. 168 (1), 99–114. Available from: https://doi.org/10.1144/0016-76492010-020.

Harmon, R.S., Halliday, A.N., Clayburn, J., Stephens, W.E., 1984. Chemical and isotopic systematics of the Caledonian intrusions of Scotland and northern England: a guide to magma source region and magma-crust interaction. Phil. Trans. R. Soc. Lond. Ser. A Math. Phys. Sci. 310 (1514), 709–742. Available from: https://doi.org/10.1098/rsta.1984.0016.

Hawkesworth, C., Cawood, P., Kemp, T., Storey, C., Dhuime, B., 2009. A matter of preservation. Science 323 (5910), 49–50. Available from: https://doi.org/10.1126/science.1168549.

Highton, A.J., 1999. Late Silurian and Devonian granitic intrusions of Scotland. In: Stephenson, D., Bevins, R.E., Millward, D., Highton, A.J., Parsons, I., Stone, P., Wadsworth, W.J. (Eds.), Caledonian Igneous Rocks of Britain, Geological Conservation Review Series. JNCC, Peterborough, pp. 397–404.

Hildebrand, R.S., Whalen, J.B., 2017. The tectonic setting and origin of Cretaceous batholiths within the north American cordillera: the case for slab failure magmatism and its significance for crustal growth. Geol. Soc. Am. Spec. Paper 532, 1–113. Available from: https://doi.org/10.1130/SPE532.

Hildebrand, R.S., Whalen, J.B., Bowring, S.A., 2018. Resolving the crustal composition paradox by 3.8 billion years of slab failure magmatism and collisional recycling of continental crust. Tectonophysics 734–735, 69–88. Available from: https://doi.org/10.1016/j.tecto.2018.04.001.

Hutton, D.H.W., McErlean, M., 1991. Silurian and early Devonian sinistral deformation of the Ratagain granite, Scotland: constraints on the age of Caledonian movements on the Great Glen fault system. J. Geol. Soc. Lond. 148, 1–4. Available from: https://doi.org/10.1144/gsjgs.148.1.0001.

Hutton, D.H.W., Stephens, W.E., Yardley, B., McErlean, M., Halliday, A.N., 1993. Ratagain Plutonic complex. In: May, F., Peacock, J.D., Smith, D.I., Barber, A.J. (Eds.), Geology of the Kintail District, Memoir of the British Geological Survey. HMSO, London, pp. 52–56.

Irvine, T.N., Baragar, W.R.A., 1971. A guide to the chemical classification of the common volcanic rocks. Can. J. Earth Sci. 8 (5), 523–548. Available from: https://doi.org/10.1139/e71-055.

Jackson, M.D., Blundy, J., Sparks, R.S.J., 2018. Chemical differentiation, cold storage and remobilization of magma in the Earth's crust. Nature 564, 405–409. Available from: https://doi.org/10.1038/s41586-018-0746-2.

Jacob, J.B., Moyen, J.F., Fiannacca, P., Laurent, O., Bachmann, O., Janoušek, V., Farina, F., Villaros, A., 2021. Crustal melting vs. fractionation of basaltic magmas: part 2, attempting to quantify mantle and crustal contributions in granitoids. Lithos 402-403, 106292. Available from: https://doi.org/10.1016/j.lithos.2021.106292.

Jacobsen, S.B., Wasserburg, G.J., 1980. Sm–Nd evolution of chondrites. Earth Planet. Sci. Lett. 50 (1), 139–155. Available from: https://doi.org/10.1016/0012-821X(80)90125-9.

Johnson, T.E., Kirkland, C.L., Viete, D.R., Fischer, S., Reddy, S.M., Evans, N.J., McDonald, B.J., 2017. Zircon geochronology reveals polyphase magmatism and crustal anatexis in the Buchan Block, NE Scotland: implications for the Grampian Orogeny. Geosci. Front. 8 (6), 1469–1478. Available from: https://doi.org/10.1016/j.gsf.2017.02.002.

Kinny, P., Strachan, R., Friend, C., Kocks, H., Rogers, G., Paterson, B., 2003. U–Pb geochronology of deformed metagranites in central Sutherland, Scotland: evidence for widespread late Silurian metamorphism and ductile deformation of the Moine Supergroup during the Caledonian orogeny. J. Geol. Soc. Lond. 160 (2), 259–269. Available from: https://doi.org/10.1144/0016-764901-087.

Krabbendam, M., Ramsay, J.G., Leslie, A.G., Tanner, P.W.G., Dietrich, D., Goodenough, K.M., 2018. Caledonian and Knoydartian overprinting of a Grenvillian inlier and the enclosing Morar Group rocks: structural evolution of the Precambrian Proto-Moine Nappe, Glenelg, NW Scotland. Scot. J. Geol. 54 (1), 13–35. https://doi.org/10.1144/sjg2017-006.

Lancaster, P.J., Strachan, R.A., Bullen, D., Fowler, M., Jaramillo, M., Saldarriaga, A.M., 2017. U–Pb zircon geochronology and geodynamic significance of 'Newer Granite' plutons in Shetland, northernmost Scottish Caledonides. J. Geol. Soc. Lond. 174 (3), 486–497. Available from: https://doi.org/10.1144/jgs2016-106.

Lara, P., Oyhantçabal, P., Dadd, K., 2017. Post-collisional, Late Neoproterozoic, high-Ba-Sr granitic magmatism from the Dom Feliciano Belt and its cratonic foreland, Uruguay: petrography, geochemistry, geochronology, and tectonic implications. Lithos 277, 178–198. Available from: https://doi.org/10.1016/j.lithos.2016.11.026.

Lawrence, A., Maffione, M., Stevenson, C.T.E., 2022. Mush ado about the Ratagain Complex, NW Scotland: insights on Caledonian granitic magmatism and emplacement from magnetic fabric analyses. Scot. J. Geol. 58 (1) https://doi.org/10.1144/sjg2021-018. Available from:

Lee, C.T.A., Morton, D.M., Kistler, R.W., Baird, A.K., 2007. Petrology and tectonics of Phanerozoic continent formation: from island arcs to accretion and continental arc magmatism. Earth Planet. Sci. Lett. 263 (3–4), 370–387. Available from: https://doi.org/10.1016/j.epsl.2007.09.025.

Leite, A.F.G.D., Fuck, R.A., Dantas, E.L., Ruiz, A.S., 2021. Appinitic and high Ba-Sr magmatism in central Brazil: insights into the late accretion stage of West Gondwana. Lithos 398-399, 106333. Available from: https://doi.org/10.1016/j.lithos.2021.106333.

Lugmair, G.W., Marti, K., 1978. Lunar initial 143Nd/144Nd: differential evolution line of the lunar crust and mantle. Earth Planet. Sci. Lett. 39 (3), 349–357. Available from: https://doi.org/10.1016/0012-821X(78)90021-3.

MacDonald, R., Fettes, D.J., 2006. The tectonomagmatic evolution of Scotland. Earth Environ. Sci. Trans. R. Soc. Edinb. 97 (3), 213–295. Available from: https://doi.org/10.1017/S0263593300001450.

Macera, P., Gasperini, D., Ranalli, G., Mahatsente, R., 2008. Slab detachment and mantle plume upwelling in subduction zones: an example from the Italian South-Eastern Alps. J. Geodyn. 45 (1), 32–48. Available from: https://doi.org/10.1016/j.jog.2007.03.004.

Maniar, P.D., Piccoli, P.M., 1989. Tectonic discrimination of granitoids. Geol. Soc. Am. Bull. 101 (5), 635–643. Available from: 10.1130/0016-7606(1989)101<0635:TDOG>2.3.CO;2.

Marshall, D., 1996. Ternplot: an excel spreadsheet for ternary diagrams. Comput. Geosci. 22 (6), 697–699. Available from: https://doi.org/10.1016/0098-3004(96)00012-X.

McDonough, W.F., Sun, S.S., 1995. The composition of the Earth. Chem. Geol. 120 (3–4), 223–253. Available from: https://doi.org/10.1016/0009-2541(94)00140-4.

McKerrow, W.S., MacNiocail, C., Dewey, J.F., 2000. The Caledonian Orogeny redefined. J. Geol. Soc. Lond. 157 (6), 1149–1154. Available from: https://doi.org/10.1144/jgs.157.6.1149.

Mendum, J.R., 2012. Late Caledonian (Scandian) and Proto-Variscan (Acadian) orogenic events in Scotland. OUGS J. 33, 37–51.

Miles, A.J., Woodcock, N.H., 2018. A combined geochronological approach to investigating long lived granite magmatism, the Shap granite, UK. Lithos 304–307, 245–257. Available from: https://doi.org/10.1016/j.lithos.2018.02.012.

Miles, A.J., Woodcock, N., Hawkesworth, C., 2016. Tectonic controls on postsubduction granite genesis and emplacement: the late Caledonian suite of Britain and Ireland. Gondw. Res. 39, 250–260. Available from: https://doi.org/10.1016/j.gr.2016.02.006.

Miller, C.F., Furbish, D.J., Walker, B.A., Claiborne, L.L., Koteas, G.C., Bleick, H.A., Miller, J.S., 2011. Growth of plutons by incremental emplacement of sheets in crystal-rich host: evidence from Miocene intrusions of the Colorado River region, Nevada, USA. Tectonophysics 500, 65–77. Available from. https://doi.org/10.1016/j.tecto.2009.07.011.

Moyen, J.F., Janoušek, V., Laurent, O., Bachmann, O., Jacob, J.B., Farina, F., Fiannacca, P., Villaros, A., 2021. Crustal melting vs. fractionation of basaltic magmas: part 1, the bipolar disorder of granite petrogenetic models. Lithos 402-403, 106291. Available from: https://doi.org/10.1016/j.lithos.2021.106291.

Neilson, J.C., Kokelaar, B.P., Crowley, Q.G., 2009. Timing, relations and cause of plutonic and volcanic activity of the Siluro-Devonian post-collision magmatic episode in the Grampian Terrane, Scotland. J. Geol. Soc. Lond. 166 (3), 545–561. Available from: https://doi.org/10.1144/0016-76492008-069.

Oliver, G.J., Wilde, S.A., Wan, Y., 2008. Geochronology and geodynamics of Scottish granitoids from the late Neoproterozoic break-up of Rodinia to Palaeozoic collision. J. Geol. Soc. Lond. 165 (3), 661–674. Available from: https://doi.org/10.1144/0016-76492007-105.

Pidgeon, R.T., Aftalion, M., 1978. Cogenetic and inherited zircon U-Pb systems in Palaeozoic granites from Scotland and England. In: Bowls, D.R., Leake, B.E. (Eds.), Crustal Evolution in Northwestern Britain and Adjacent Regions. Seal House Press, Liverpool, pp. 183–220.

Read, H.H., 1961. Aspects of Caledonian magmatism in Britain. Geol. J. 2 (4), 653–683. Available from: https://doi.org/10.1002/gj.3350020408.

Rock, N.M.S., Gaskarth, J.W., Henney, P.J., Shand, P., 1988. Late Caledonian dyke swarms of northern Britain; some preliminary petrogenetic and tectonic implications of their province-wide distribution and chemical variation. Can. Mineral. 26 (1), 3–22.

Rogers, G., Dunning, G.R., 1991. Geochronology of appinitic and related granitic magmatism in the W Highlands of Scotland: constraints on the timing of transcurrent fault movement. J. Geol. Soc. Lond. 148, 17–27. Available from: https://doi.org/10.1144/gsjgs.148.1.0017.

Rudnick, R., 1995. Making continental crust. Nature 378, 571–578. https://doi.org/10.1038/378571a0.

Searle, M.P., 2022. Tectonic evolution of the Caledonian orogeny in Scotland: a review based on the timing of magmatism, metamorphism and deformation. Geol. Mag. 159 (1), 124–152. Available from: https://doi.org/10.1017/S0016756821000947.

Soper, N.J., 1986. The Newer Granite problem: a geotectonic view. Geol. Mag. 123 (3), 227–236. Available from: https://doi.org/10.1017/S0016756800034725.

Sparks, R.S.J., Annen, C., Blundy, J.D., Cashman, K.V., Rust, A.C., Jackson, M.D., 2019. Formation and dynamics of magma reservoirs. Phil. Trans. R. Soc. A 377 (2139), 20180019. Available from: https://doi.org/10.1098/rsta.2018.0019.

Steiger, R.H., Jäger, E., 1977. Subcommission on geochronology: convention on the use of decay constants in geo- and cosmochronology. Earth Planet. Sci. Lett. 36 (3), 359–362. Available from: https://doi.org/10.1016/0012-821X(77)90060-7.

Stephens, W., Halliday, A., 1984. Geochemical contrasts between late Caledonian granitoid plutons of northern, central and southern Scotland. Earth Environ. Sci. Trans. R. Soc. Edinb. 75 (2), 259–273. https://doi.org/10.1017/S0263593300013894.

Stephenson, D., Bevins, R.E., Millward, D., Stone, P., Parsons, I., Highton, A.J., Wadsworth, W.J., 1999. Caledonian Igneous Rocks of Great Britain. JNCC, Peterborough.

Stevenson, C., Hutton, D., Price, A., 2008. The Trawenagh Bay Granite and a new model for the emplacement of the Donegal Batholith. Earth Environ. Sci. Trans. R. Soc. Edinb. 97 (4), 455–477. https://doi.org/10.1017/S0263593300001565.

Strachan, R.A., Alsop, G.I., Ramezani, J., Frazer, R.E., Burns, I.M., Holdsworth, R.E., 2020. Patterns of Silurian deformation and magmatism during sinistral oblique convergence, northern Scottish Caledonides. J. Geol. Soc. London 177 (5), 893–910.

Streckeisen, A., 1976. To each plutonic rock its proper name. Earth-Sci. Rev. 12 (1), 1–33. Available from: https://doi.org/10.1016/0012-8252(76)90052-0.

Sun, S.-S., McDonough, W.F., 1989. Chemical and isotopic systematics of oceanic basalts: implications for mantle composition and processes. Geol. Soc. Lond. Spec. Publ. 42, 313–345. Available from: https://doi.org/10.1144/GSL.SP.1989.042.01.19.

Tarney, J., Jones, C.E., 1994. Trace element geochemistry of orogenic igneous rocks and crustal growth models. J. Geol. Soc. Lond. 151 (5), 855–868. Available from: https://doi.org/10.1144/gsjgs.151.5.0855.

Thirlwall, M.F., 1981. Implications for Caledonian plate tectonic models of chemical data from volcanic rocks of the British Old Red Sandstone. J. Geol. Soc. Lond. 138 (2), 123–138. Available from: https://doi.org/10.1144/gsjgs.138.2.0123.

Thirlwall, M.F., 1982. Systematic variation in chemistry and Nd-Sr isotopes across a Caledonian calc-alkaline volcanic arc: implications for source materials. Earth Planet. Sci. Lett. 58 (1), 27–50. Available from: https://doi.org/10.1016/0012-821X(82)90101-7.

Thirlwall, M.F., 1988. Geochronology of late Caledonian magmatism in northern Britain. J. Geol. Soc. Lond. 145 (11), 951–967. Available from: https://doi.org/10.1144/gsjgs.145.6.0951.

Thirlwall, M.F., Burnard, P., 1990. Pb-Sr-Nd isotope and chemical study of the origin of undersaturated and oversaturated shoshonitic magmas from the Borralan pluton, Assynt, NW Scotland. J. Geol. Soc. Lond. 147 (2), 259–269. Available from: https://doi.org/10.1144/gsjgs.147.2.0259.

Thompson, R.N., Fowler, M.B., 1986. Subduction-related shoshonitic and ultrapotassic magmatism: a study of Siluro-Ordovician syenites from the Scottish Caledonides. Contrib. Mineral. Petrol. 94, 507–522. Available from: https://doi.org/10.1007/BF00376342.

Troll, V.R., Emeleus, H., Nicoll, G.R., Mattsson, T., Ellam, R., Donaldson, C.H., Harris, C., 2019. A large explosive silicic eruption in the British Palaeogene Igneous Province. Sci. Rep. 9, 494. Available from: https://doi.org/10.1038/s41598-018-35855-w.

Turnell, H.B., 1985. Palaeomagnetism and Rb-Sr ages of the Ratagan and Comrie intrusions. Geophys. J. Int. 83, 363–378. Available from: https://doi.org/10.1111/j.1365-246X.1985.tb06492.x.

Watson, J., 1984. The ending of the Caledonian orogeny in Scotland. J. Geol. Soc. Lond. 141 (2), 193–214. Available from: https://doi.org/10.1144/gsjgs.141.2.0193.

Whalen, J.B., Hildebrand, R.S., 2019. Trace element discrimination of arc, slab failure, and A-type granitic rocks. Lithos 348–349, 105179. Available from: https://doi.org/10.1016/j.lithos.2019.105179.

Whitney, D.L., Evans, B.W., 2010. Abbreviations for names of rock-forming minerals. Am. Mineral. 95, 185–187. Available from: https://doi.org/10.2138/am.2010.3371.

Woodcock, N.H., Soper, N.J., Miles, A.J., 2019. Age of the Acadian deformation and Devonian granites in northern England: a review. Proc. Yorkshire Geol. Soc. 62, 238–253. Available from: https://doi.org/10.1144/pygs2018-009.

Ye, H.-M., Li, X.-H., Li, Z.-X., Zhang, C.-L., 2008. Age and origin of high Ba–Sr appinite–granites at the northwestern margin of the Tibet Plateau: Implications for early Paleozoic tectonic evolution of the Western Kunlun orogenic belt. Gondw. Res. 13 (1), 126–138. Available from: https://doi.org/10.1016/j.gr.2007.08.005.